GENERALIZED PREFERENTIAL FLOW MODEL VALIDATION USING FIELD-SCALE DATA

A Thesis

Presented to the Faculty of the Graduate School

of Cornell University

In Partial Fulfillment of the Requirements for the Degree of

Master of Science

by

Ian Christopher Toevs

January 2007

ABSTRACT

The challenge in predicting the movement of pesticides and other solutes in soil that exhibits preferential flow conditions is due to the variability in solute velocity through different flow paths. The generalized preferential flow model (GPFM) is a closed form solution to the convective dispersive equation, which combines these different flow paths into multiple groups (i.e. pore groups) with varying properties. The properties that vary between pore groups are limited to the solute velocity, dispersion coefficient, and the contribution to the solute transport. By using the GPFM to predict the solute transport in each pore group, it is possible to obtain an average concentration at any point in the soil profile. However, the GPFM lacks significant field-scale validation.

In order to examine the viability of the GPFM, the predicted results of the model were compared to measured field-scale data. The measured data used to validate the GPFM was from field scale experiments by Gish et al. (2004) and Kung et al. (2000b and 2005). The experiments used conservative tracers, applied at the soil surface, and collected in the discharge of an underground drainage tile. One of these experiments took place at the Walworth County Farm in Elkhorn, Wisconsin and was a long duration, steady state experiment that revealed nearly the entire solute breakthrough at different irrigation rates. The other experiment was conducted at the South East Purdue Agricultural Center (SEPAC) in Butlerville, Indiana and was a short duration, transient flow situation in which tracers were sequentially applied during one experiment.

In order to compare the results of the GPFM with the measured data, modifications were made to the model output to achieve a similar unit to that of the measured data. While modeling the transient flow experiments, other modifications were found to be necessary in order to model a transient process using steady state pieces. The modeling results from the steady state experiment show similar mass recovery rates with differences from the measured data of not more than 5% when the measured results were not affected by external circumstances. The transient flow results were significantly influenced by the water hydrograph for the system but were able to capture the trend of the solute leaching. These results show potential for further implementation of the model. The next step to be addressed is how to measure or systematically specify the modeling parameters.

BIOGRAPHICAL SKETCH

Ian Toevs, the eldest of three children born to loving parents, grew up in the farming country of Southeastern Idaho. Through working on his grandfather's farm and at his father's irrigation and implement dealership, Ian developed an interest in agriculture. The love and encouragement from his parents taught and inspired him to do all things full-heartedly and to put others first. These skills helped Ian to successfully complete an undergraduate degree in Agricultural Engineering at the University of Idaho. While at the U of I, Ian developed an interest in water resources and also studied Outdoor Recreation Leadership (a great way to take classes that involved his hobbies). There he earned a bachelor of science degree in Agricultural Engineering along with an Outdoor Recreation minor. Ian met his future bride at the University of Idaho and a month after their May 2004 graduation they were married. This was followed by a move to Ithaca, New York two weeks after the wedding to attend Cornell University. Attending Cornell was an educational and enlightening experience for Ian in both engineering and life. Ian is now working at a civil and environmental engineering consulting firm in Syracuse, New York.

To my wonderful wife and friend Vanessa.

ACKNOWLEDGMENTS

Special thanks to Dr. K.J. Samuel Kung for supplying the data and wonderful advice for this work. Additional acknowledgment is due to Dr. Timothy J. Gish and the contributing authors to Dr. Kung's work: G. Bubenzer, M. Hanke, C.S. Helling, E.J. Kladivko, D.C. Perry, and J. Posner.

I want to especially thank Tammo Steenhuis, for providing the motivation, encouragement, and direction when it was most needed and facilitating a place of study that is challenging and rewarding. My other committee member, Larry Cathles, was also a great help in refining this work and guiding my course of study.

My wife Vanessa provided much needed support and motivation and I am very appreciative of this. Lastly and most importantly I would like to thank my parents for setting such an amazing example for me and instilling values that have become the base of my belief system and life philosophy.

TABLE OF CONTENTS

LIST OF FIGURES

LIST OF TABLES

LIST OF ABBREVIATIONS

GPFM: generalized preferential flow model

DZ: distribution zone

CZ: conveyance zone

BTC: breakthrough curve

PG: pore group

S1: the designation of the modeling scenario primarily fit to the results for the low irrigation rate experiment at SEPAC

S2: the designation of the modeling scenario primarily fit to the results for the middle irrigation rate experiment at SEPAC

S3: the designation of the modeling scenario primarily fit to the results for the high irrigation rate experiment at SEPAC

LIST OF SYMBOLS

C [$M\ L^{-3}$]: solute concentration; mass of chemical per volume of water

C_o [$M\ L^{-3}$]: initial solute concentration applied at the soil surface

C_i [$M\ L^{-3}$]: solute concentration in pore group *I*

C_A [$M\ L^{-3}$]: average solute concentration in the soil profile (from all of the contributing pore groups)

a_i [unitless]: contribution factor (percentage) of pore group *I* to the average solute concentration

J'_i [$M\ T^{-1}\ L^{-2}$]: mass flux per unit area through pore group *I*

J_T [$M\ T^{-1}$]: total mass flux from the drain tile discharge

q_i [$L\ T^{-1}$]: water flux through pore group *I*, the volumetric flow normalized (divided) by the area contributing to the flow

I_r [$L\ T^{-1}$]: irrigation rate of water at the surface of the soil

x_d [L]: depth of the distribution zone

x_c [L]: depth of the conveyance zone

x_T [L]: depth of modeled solute concentration in the soil profile ($x_d + x_c$)

w [L]: depth of water in the distribution zone; obtained by multiplying the depth of the distribution zone by the moisture content of the distribution zone

η [T^{-1}]: the irrigation rate divided by the depth of water in the distribution zone (I_r/w)

t [T]: time series from the commencement of the experiment

t_{pi} [T]: time series for pore group *I*

$_{acti}$ [T]: time (after the beginning of the experiment) of pore group *I* activation

t_{th} [T]: time series for tracer *h*

$_{aph}$ [T]: time (after the beginning of the experiment) of tracer *h* application

v_i [L T^{-1}]: solute velocity in a specific pore group

D_i [L^2 T^{-1}]: solute dispersion in a specific pore group

n [unitless]: number of pore groups

I [unitless]: pore group counter

h [unitless]: tracer counter

$_D$ [L^3 L^{-3}]: moisture content of the distribution zone

$_i$ [L^3 L^{-3}]: boundary moisture content (constant) of pore group *I*

[L^3 L^{-3}]: average moisture content of the soil profile

k_i [L T^{-1}]: conductivity of pore group *I* at the observed moisture content of the soil profile

K_i [L T^{-1}]: conductivity of pore group *I* at the boundary moisture content

A_a [L^3]: area of tracer application

A_d [L^3]: contributing area to the drainage tile of interest

m_s [M]: mass of solute applied

INTRODUCTION

Contaminants that leach below the root zone pose a potentially serious threat to public health by polluting shallow groundwater (e.g. cisterns, springs, shallow wells), migrating into deeper groundwater (e.g. deep wells), and possible exfiltration back to surface water from an aquifer (Wycisk et al., 2003). These three sources of water contribute to the drinking water for the entire world. Our dependence on safe, clean drinking water emphasizes the need for an accurate understanding of the processes that affect water contamination.

As the processes of contaminant transport are identified and studied it is essential to develop accurate models that are easy to use and require modest and obtainable data inputs. Numerically defining transport processes helps to identify scenarios that may lead to subsurface contamination as well as accommodate more cost effective strategies in the assessment and remediation of contaminated areas. However, there are many challenges in modeling contaminant transport. The primary challenge is that which is caused by the rapid and non-uniform transport of water and contaminants in the subsurface (Stagnitti et al., 1994). Virtually all field soils have been shown to exhibit some level of this preferential flow (Dekker and Ritsema, 1994). Soil macropores are one type of pathway for preferential flow (Beven and Germann, 1982). These pathways develop in the soil as a result of interaggregate pore spaces, roots, faunal tunnels, and shrink-swell cracks (Skopp, 1981). Although preferential flow occurs under many conditions in nearly all soil types, the extent and magnitude is difficult to estimate. In other words preferential flow is seen as predictably unpredictable.

Numerous studies have shown the evidence of preferential flow in both lab and field scale experiments. This occurrence was addressed as early as 1882 by Lawes et al. and has been the focus of much research since the 1970's (Hill and Parlange, 1972; Raats, 1973; Philip, 1975; and Parlange and Hill, 1976). Richard and Steenhuis (1988) examined the effects of preferential flow by sampling the discharge from buried, perforated pipes that serve to drain the moisture from the soil profile. These underground pipes are known as drain tiles. Other recent studies have utilized these drain tiles to obtain field scale breakthrough curves Kung et al., 2000a; Kung et al., 2000b; Jaynes et al., 2001; Buelke et al., 2001; Fox et al., 2004; Gish et al., 2004; and Kung et al., 2005). These studies have documented the remarkable speed at which solutes can migrate to drain tiles. In Indiana, Kung et al. (2000b) found that tracers reached a drain tile, buried approximately 1 m below the soil surface, between 12 and 18 min after application. Gish et al. (2004) reported nearly identical results in Wisconsin. Improved methodology (as discussed in Kung et al., 2000b; Hanke et al., 2004; Gish et al., 2004; and Kung et al. 2005) in sampling and experimental design helped to “see” these processes. The overall results of the improved methods were an increased mass recovery (caused by a high irrigation rate over a large area to drive the solute towards the monitored drain tile) and isolating the field-scale transport processes through reducing variability due to climatic conditions or irrigation rates (accomplished by maintaining a constant, high irrigation rate outside- and an independent irrigation rate inside the area of tracer application). Monitoring chemical breakthrough in drain tile effluent (as opposed to lysimeters or soil cores) has also enhanced the ability to capture the significance (i.e. arrival times, magnitude of peaks, etc.) of the cumulative impacts of preferential flow.

This improvement in field scale data collection is extremely helpful in model development and validation.

Existing Models

Numerous models for predicting solute transport in the soil currently exist; however, there is still a significant need for model validation (Feyen et al., 1998). These approaches typically use some form of Richard's equation for water flow (such as the analytical solution by Parlange, 1972) and the convective-dispersive equation for solute transport (van der Molen, 1956). Often to account for preferential flow these models implement a two-domain concept for micro- and macro- porous flow (Skopp et al., 1981; Haws et al., 2004; and Larsbo et al., 2005). Steenhuis et al. (1988) and Steenhuis et al. (1990) proposed a piecewise linear conductivity function to predict water and solute flow laterally in a hillslope and vertically through the soil profile, respectively. This model used a multi-domain approach. Each domain has its own velocity derived from the piecewise linear approximation to the hydraulic conductivity curve of a given soil. Durner and Flühler (1996) followed these techniques and found that a higher number of domains resulted in better predicted breakthrough curves. They also proposed investigating a continuous pore-size distribution model and raised the question about multi-domain models in transient flow. Kung et al. (2005) directly addressed this question with his pore spectrum model. This helped to better understand the soil conductivity and its variation by classifying the pore size spectrum and the frequency of occurrence for a continuous range of pore sizes with a sharp cutoff at either end of the pore size spectrum (<1 nm and >0.1 m). An advantage of this model is the demonstrated similarities between different

soils, which may allow measurements taken at a certain location to be transferred to other sites through modeling parameter relationships. Kung used measurements of solute transport in a soil to empirically derive the parameters for his pore spectrum equation from the breakthrough curves of a field scale tracer flow study. With a known pore spectrum it is possible to model the solute transport in the soil by assuming the individual soil pores behave as capillary tubes. One challenge of this approach is in developing a discrete number of pore groups each with an effective size or velocity. The number of domains required to adequately characterize the behavior of a soil, remains a primary unknown variable.

The Generalized Preferential Flow Model (GPFM) was proposed by Kim et al. (2005) and used one of the analytical solutions presented in Toride et al. (1995). This is a multi-domain method based on the convective-dispersive equation. The GPFM is a closed form solution that can be implemented in nearly any computerized numerical application or used as a back-of-the-envelope approximation, which makes it appealing to use independently or for inclusion in more complex models. The concept of the GPFM has been demonstrated by Kim and others and Darnault et al. (2004) but not validated with field-scale experiments. The focus of this work is to show that the GPFM can effectively model field-scale solute transport. Additionally, it will provide general insight into the number of pore groups necessary to classify a continuous spectrum of pores.

Generalized Preferential Flow Model Conceptualization

In the GPFM the soil profile is conceptually divided horizontally into two components- the distribution zone and the conveyance zone. The distribution

zone is the uppermost layer of soil and its depth is controlled by land use and tillage practices. The conveyance zone lies below the distribution zone and typically exhibits a less uniform solute distribution through multiple pore groups with varying solute velocities. Figure 1 shows a schematic diagram of the GPFM. When Figure 1 is compared with the picture in Figure 2 many similarities are seen.

Figure 2 shows an experiment in which a blue dye tracer was applied at the soil surface and allowed to infiltrate into the soil. A hole was then dug to expose the stained soil profile. Figure 2 reveals that the upper layer (distribution zone) of the soil profile is uniformly stained. Directly below the uniformly stained area the tracer traveled downward to many different depths. The shallower depths indicate slower solute velocities while smaller preferential flow paths, or pore groups, are seen extending far past the uniformly stained area, indicating very high velocities. The conveyance zone consists of the soil profile below the distribution zone as shown in Figure 2.

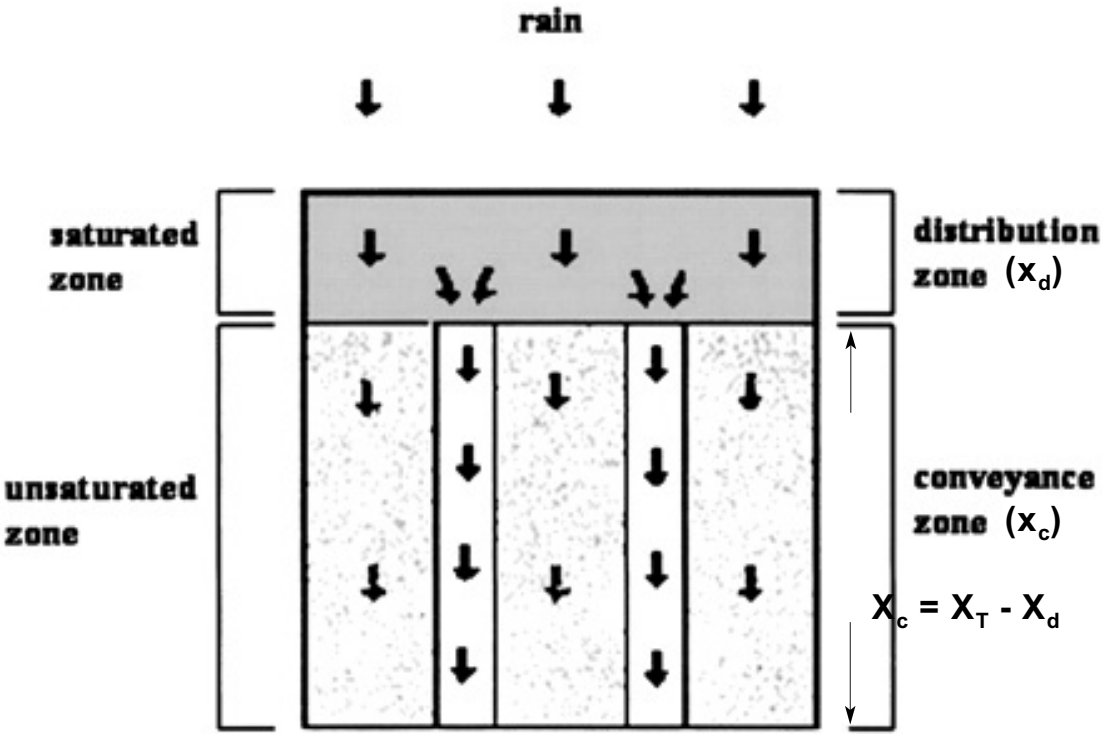

Figure 1: A conceptual diagram of the modeling approach in the Generalized Preferential Flow Model. The arrows show the flow of the water (and solute) from the distribution zone being partitioned to different flow paths in the conveyance zone. The depth of the distribution zone (x_d), the conveyance zone (x_c), the total depth to the drain tile or point of interest (x_T), as well as the relationship between the three are also shown.

Figure 2: An experiment using a blue dye tracer that reveals the distribution zone and conveyance zone in an undisturbed soil profile.

The distribution zone acts as a linear reservoir, which is mathematically similar to a situation where the applied solute is mixed in the distribution zone with the uniform rainfall and distributed into the preferential and matrix flow paths of the deeper soil. The behavior of the distribution zone when the initial solute concentration in the distribution zone is C_o [M L^{-3}] and the rainfall or irrigation is solute free is described by:

$$C(x,t) = C_0 \exp\left(-\frac{I_r}{w}t\right) \qquad x = x_d \qquad t > 0 \qquad (1a)$$

$$C(x,t) = 0 \qquad x \rightarrow \infty \qquad t > 0 \qquad (1b)$$

$$C(x,t) = 0 \qquad x > x_d \qquad t = 0. \qquad (1c)$$

Here, t [T] is the time of solute application, I_r [L T^{-1}] is the irrigation rate, and w [L] is the depth of water in the distribution zone (see Figure 3). The term w is calculated by multiplying x_d [L] (the depth of the distribution zone) by the moisture content of the distribution zone. In order to calculate C_o the mass of solute applied is divided by the volume of water in the distribution zone, which is equivalent to the area of application (A_a) multiplied by w. Figure 3 shows a cross section of the distribution zone. When applied as a short pulse, the tracer is assumed to rapidly and uniformly mix with the water in the distribution zone.

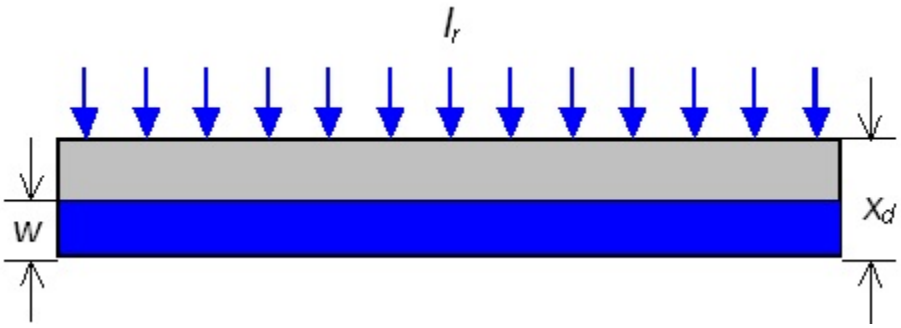

Figure 3: Cross sectional view of the distribution zone showing the irrigation rate at the soil surface (I_r), the depth of the distribution zone (x_d), and the depth of water in the distribution zone (w).

The result of Equation 1a is a concentration of solute (as a function of time) that is released into the conveyance zone. Once the solute has been routed from the distribution zone into the conveyance zone, the solute is modeled in each pore group using the convective-dispersive equation. The convective-dispersive equation, as shown below, is often used to predict the transport of solutes in the soil:

$$D\frac{\partial^2 C}{\partial x^2} - v\frac{\partial C}{\partial x} = \frac{\partial C}{\partial t} \quad . \tag{2}$$

Here the velocity, v [L T^{-1}], is the solute velocity and D [L^2 T^{-1}] is a measure of the solute dispersion. Typically when using the convective-dispersive equation for vertical one-dimensional flow, the average solute velocity is fit to facilitate the imposed water flux. However, the assumption that there exists multiple pore groups (with different solute velocities and amounts of water flowing through them) makes it possible to model both matrix- and preferential- flow. This is implemented by specifying velocities and water fluxes for each pore group that add to meet the total imposed flux of rainfall or irrigation.

The equation used in the GPFM was originally derived by Toride et al. (1995) from Eq. 2 using the boundary conditions in Eq. 1a, 1b, and 1c. This equation models the solute concentration in an individual pore group (denoted by the subscript *I*) of a semi-infinite column of porous media. As shown by Kim et al. (2005) the solution is

$$C_i(x_c,t) = \frac{1}{2} C_o \exp\left(-\frac{I_r}{w} t\right) \left\{ \begin{array}{l} \exp\left[\frac{v_i x_c}{2 D_i}\left(1-\alpha_i\right)\right] erfc\left(\frac{x_c - v_i t \alpha_i}{2\sqrt{D_i t}}\right) \\ + \exp\left[\frac{v_i x_c}{2 D_i}\left(1+\alpha_i\right)\right] erfc\left(\frac{x_c + v_i t \alpha_i}{2\sqrt{D_i t}}\right) \end{array} \right\} \quad (3)$$

where x_c [L] is the depth of the drain tile below the distribution zone and

$$\alpha_i = \sqrt{1 - \frac{4 D_i I_r}{w v_i^2}}. \quad (4)$$

Equation 4 (thus Eq. 3) is valid as long as it satisfies the following relation:

$$\frac{4 D_i I_r}{w v_i^2} < 1. \quad (5)$$

When x_c and t are sufficiently large (i.e. $(x_c + v_i t \quad _i)/(4 D_i t)^{½} > 3$) the last term of Eq. 3 can be neglected.

Figures 1 and 2 show that the solute released from the distribution zone is routed into a number of pore groups in the conveyance zone. These pore groups are delineated by the moisture content of the soil profile. If we consider a completely dry, structured soil profile the smallest radius pore group will hold the first moisture applied to the soil- a result of the high suction in the small pores. As the soil profile continues to fill with water and the small radius pores reach capacity, additional pore groups will become “active” (i.e. begin to absorb water). This occurs when the pore group reaches its boundary moisture content. The boundary moisture content (denoted by $_i$ for

pore group *I*) is the average moisture content of the entire soil profile at the time when a pore group reaches capacity and the next pore group begins to soak up some of the infiltrating water. As the pore groups absorb incoming water they will begin to transport water if the suction of the pores is lower than the pressure and gravity induced gradient.

When using Equations 3 and 4 as shown above, the average concentration is found by summing the calculated concentration from each pore group, weighted by the fraction of the total contribution:

$$C_A = \sum_{i=0}^{n} a_i C_i . \qquad (6)$$

This equation yields the average concentration C_A [M L^{-3}] at time t and depth x_c, C_i [M L^{-3}] is the concentration in pore group I at time t and depth x_c. The contribution factor (a_i) is the proportion of the concentration that a pore group accounts for, and n is the number of pore groups through which water flows. However, when monitoring solute transport by observing drain tile discharge, the concentration in the tile line is different than given by Eq. 6. This is because more water enters the tile line than passes through the narrow band of tracer application. Hence the concentration expressed in Eq. 6 is diluted by an unknown amount. Therefore, the total mass of solute leached from the soil into the tile line is typically reported as a mass flux- a measurement independent of the dilution. To calculate the mass flux in the tile line we first multiply the calculated concentration from a pore group (C_i [M L^{-3}]) by the water flux through the pore group (q_i [L^3 T^{-1} L^{-2}]). Thus C_i from Eq. 3 becomes J_i' [M T^{-1} L^{-2}], the mass flux per unit area, as shown by:

$$J_i'(x_c,t) = \frac{1}{2} C_o q_i \exp\left(-\frac{I_r}{w} t\right) \left\{ \begin{array}{l} \exp\left[\frac{v_i x_c}{2D_i}(1-\alpha_i)\right] erfc\left(\frac{x_c - v_i t \alpha_i}{2\sqrt{D_i t}}\right) \\ + \exp\left[\frac{v_i x_c}{2D_i}(1+\alpha_i)\right] erfc\left(\frac{x_c + v_i t \alpha_i}{2\sqrt{D_i t}}\right) \end{array} \right\} \quad (7)$$

The water flux in the pore groups, as used in Eq. 7, is calculated as follows: When the upper boundary moisture content, θ_i, is less than the average moisture condition in the soil, Θ, then the pore group is flowing full and the flux, q_i, can be calculated as

$$q_i = v_i (\theta_i - \theta_{i-1}) \text{ for } \quad \Theta > \theta_i . \quad (8)$$

The water flux can also be calculated when the pore group is flowing partially full (i.e. the moisture content is between the upper and lower boundary moisture contents):

$$q_i = v_i (\Theta - \theta_{i-1}) \quad \text{for} \quad \theta_{i-1} < \Theta < \theta_i. \quad (9)$$

There is no flux in a pore group when the moisture content is less than the boundary moisture content, as shown by:

$$q_i = 0 \quad \text{for} \quad \Theta < \theta_{i-1}. \quad (10)$$

Mass balance consideration, of course, dictate that:

$$\sum_{i=0}^{n} q_i = I_r \quad (11)$$

which is valid under steady state conditions throughout the column. In a transient flow situation the sum of water flux at $x_c = 0$ is equal to the irrigation rate minus what is absorbed when wetting the distribution zone:

$$\sum_{i=0}^{n} q_i = I_r - \frac{dw}{dt}. \quad (12)$$

The mass flux in the tile line can now be obtained by simply summing the mass flux per unit area of each pore group and multiplying by the area over which the solutes are applied:

$$J_T = A_a \sum_{i=0}^{n} J_i' \tag{13}$$

The concentration in the tile line under a steady state condition can be predicted by the quotient of the mass flux and the amount of water that falls on the contributing area of the tile line at time *t*:

$$C = \frac{J_T}{A_d I_r} \tag{14}$$

where A_d [L^2] is the contributing area of the tile line.

The challenge in achieving reasonable results when modeling solute transport in the conveyance zone relates to the variation in pore sizes and their frequency of occurrence. Kung et al. (2005) pointed out that "natural soils have a spectrum of pores with radii generally ranging from 10^{-3} to 10^{-7} m." Additionally, Kung and others found, through his pore spectrum model, that a 0.44 cm hr^{-1} irrigation rate caused >10^9 pores m^{-2} with approximate radii of 1 m and <1 pore m^{-2} with radii larger than 20 m to be active. This was at the Walworth County Farm in Elkhorn, WI where the soil is a Pella silt loam (fine-silty, mixed, superactive, mesic, Typic Endoaquolls) and the irrigation rate was at a maximum without causing ponding on the surface. Given this information, the GPFM translates the variability in soil pores into multiple domains (i.e. effective pore groups), each having a different velocity and contribution to the total water flux.

Site Description

Data used in testing and validating the GPFM came from two tile drained no-till field plots throughout the Midwestern United States. These locations were the Walworth County Farm in Elkhorn, Wisconsin (Gish et al., 2004 and Kung et al., 2005) and the South East Purdue Agricultural Center (SEPAC)

in Butlerville, Indiana (Kung et al., 2000b). Table 1 shows a comparison of the soil types at these sites.

Table 1: Comparison of soil properties for the three field sites. The saturated moisture content of the soil is represented by θ_s.

Field site	Soil classification	Soil layer depth (cm)	θ_s ($cm^3\ cm^{-3}$)	Soil layer description
Walworth, WI	Pella silt loam: fine-silty, mixed, mesic Typic Endoaquolls.	0-35	0.45	silt loam
		35-65		clay-loam, sandy clay-loam
		65-80~130		glacial well-mixed gravelly till
		>80~130		compacted glacial till
SEPAC, IN	Clermont silt loam: fine-silty, mixed, superactive, mesic Typic Glossaqualfs.	0-30	0.44	silt loam
		30-45		silt loam
		45-96		silt loam
		96-126		loam/silt loam

Walworth, WI: Steady State Experiments

The data used for modeling the experiments at the Walworth site are shown in Table 2. These experiments were conducted for a long duration (22 days or more) under steady state conditions. The center tile line was monitored for solute flux and bordering tile lines were spaced 18 m on either

side. In each experiment a large (32m X 30m) surrounding area was irrigated at 0.4 cm hr^{-1} in order to maintain a relatively steady water table height. The tracers were applied inside a specially designed shed (offset from tile line by 0.3 m) with an independent irrigation rate. These methods follow the Kung partial area flux approach. The shed and irrigation apparatus used at this site are described in more detail by Hanke et al. (2004), Gish et al. (2004), and Kung et al. (2005). The highest irrigation rate used within the shed for these experiments was 0.44 cm hr^{-1} (Gish et al., 2004). This was reported to be the highest possible without causing ponding at the soil surface. Gish and others used one shed 3.5- by 24- m for tracer (bromide) application, while Kung and others used two of these sheds. Irrigation rates used by Kung and others were 0.12 cm hr^{-1} (for pentafluorobenzoic acid (PFBA)) and 0.24 cm hr^{-1} (for two experiments, one using PFBA and the other o-trifluoromethylbenzoic acid (o-TFMBA)). These were the only steady state experiments selected for model validation.

Figure 4 shows the plan view of the Walworth site and Figure 5 shows a cross sectional view. These figures show the tracer applied area and its approximate location compared to the irrigation lines and the drain tiles. Figure 5 also shows the shed that contains the entire area of tracer application and is where the irrigation rate was varied for the three Walworth experiments while the surrounding area was irrigated at a constant rate.

Table 2: Experimental setup at the Walworth field site showing the irrigation rate (I_r), tracer applied, spacing of the drain tiles, total depth (x_T) to drain tile, mass of tracer applied (m_s), area of tracer application (A_a), and the irrigated area.			
I_r (cm hr^{-1})	0.12	0.24	0.44
Tracer	PFBA	PFBA	Br
Pre-experiment preparation	applied tracer two days after tile discharge reached steady state		
Duration of irr. (days)	25	25	22
Tile spacing (m)	18		
x_T (cm)	95		
m_s (g)	1000	686	2350
A_a (m x m)	2 x (3.5 x 24)	2 x (3.5 x 24)	1 x (3.5 x 24)
Irrigated area (m x m)	32 x 30		

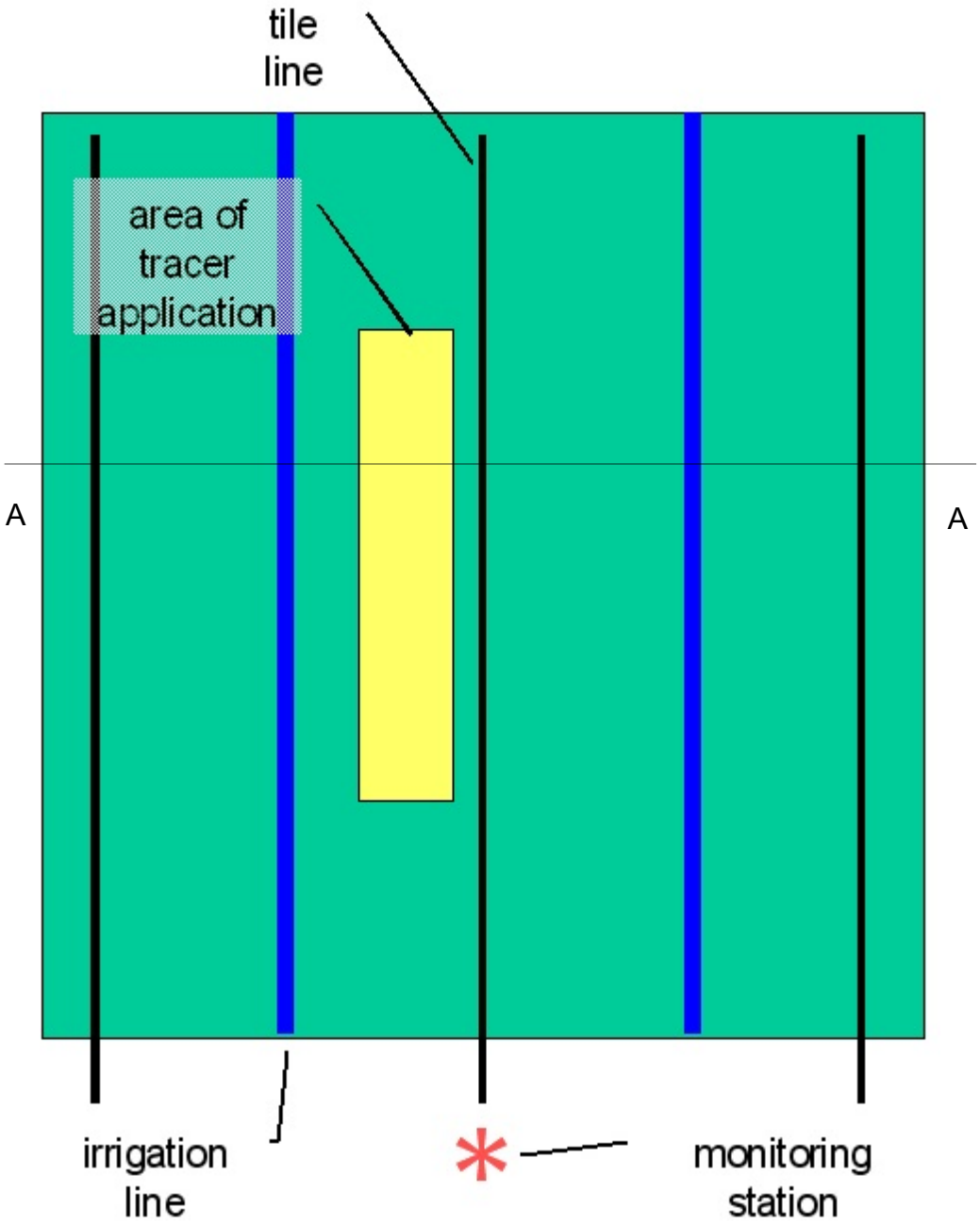

Figure 4: Diagram of the experimental setup at the Walworth field site showing the area of tracer application with respect to the irrigation and drain tile lines. The drain tile line marked with an asterisk was monitored for tracer breakthrough.

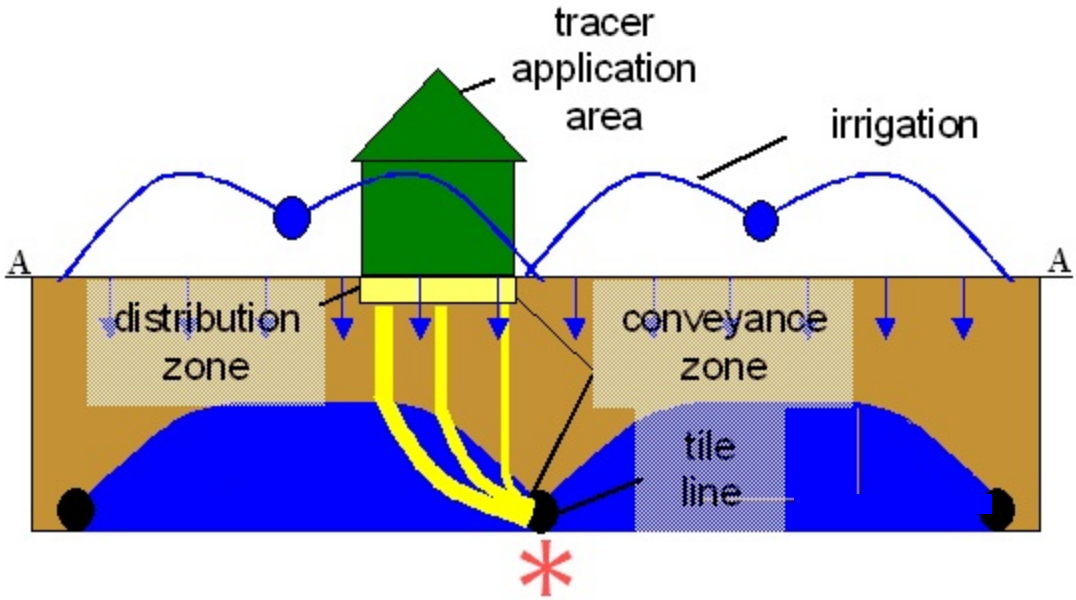

Figure 5: The cross sectional view of section A (shown in Figure 4) of the setup at Walworth. This figure shows the shed that the tracer was applied in and the approximate water table which caused the tracer to migrate towards the center drain tile line. The distribution zone and conveyance zone are also called out on this figure.

SEPAC, IN: Transient Flow, Sequentially Applied Tracers

The experiment at SEPAC (Kung et al., 2000b) was conducted as a typical low-intensity, long-duration rainstorm, using an irrigation rate of 0.3 cm hr^{-1} for 10 hrs. The data used for modeling are shown in Table 3. This experiment also used the Kung partial area flux approach. The drain tiles at the SEPAC site were spaced on 10 m intervals. In this experiment the entire area (24 m x 60 m) was irrigated at the same rate and the tracers were applied to a small area (1.5 m x 24 m) slightly offset (0.3 m) from the center drain tile. The tracer application scheme involved applying the first tracer (bromide (Br^-)) at the commencement of irrigation (t = 0 hrs) and applying each sequential tracer (PFBA, o-TFMBA, and 2,6-difluorobenzoic acid (2,6-DFBA)) at two hour intervals through t = 6 hrs. This experiment showed dramatically decreasing arrival times of the tracers, which was an indicator of increasing preferential flow (pore water velocity).

Figures 4 and 5 are also representative of the SEPAC experimental setup. The main differences between the two experiments is that there was no shed in which the tracer was applied and the entire site received the same irrigation rate. A procedural differences was in the sequential (during the same experiment) tracer application as opposed to individual experiments for each tracer and irrigation rate at Walworth.

Table 3: Experimental setup at the SEPAC site showing the irrigation rate (I_r), tracer applied, spacing of the drain tiles, total depth (x_T) to drain tile, mass of tracer applied (m_s), time of tracer application after the beginning of the experiment ($_{aph}$), area of tracer application (A_a), and the irrigated area.

I_r (cm hr^{-1})	0.3			
Tracer	Br	PFBA	o-TFMBA	2,6-DFBA
Pre-experiment preparation	1.2 cm irrigation 2 days prior to commencement of experiment			
Duration of irr. (hrs)	10			
Tile spacing (m)	10			
x_T (cm)	90			
m_s (g)	1930	1370	1500	1500
$_{aph}$ (hrs)	0	2	4	6
A_a (m x m)	1.5 x 24			
Irrigated area (m x m)	24 x 60			

Model Implementation

Two sets of parameters were used to model the solute leached through the soil profile and into drain tiles using the GPFM. These two groups of parameters consist of those that were initially set and remained constant throughout a modeling scenario and the fitting parameters, which were adjusted to achieve the best agreement between the modeled and measured data. The initial parameters include overall time (t), depth below the ground surface at which the solute concentration is modeled (x_T), the depth of the distribution zone (x_d), depth of the conveyance zone (x_c), depth of the water in the distribution zone (w), area of tracer application (A_a) as well as the area contributing to the drain tile (A_d), and the irrigation rate (I_r). These parameters were specified or determined from the following information: The experimental procedures were used to determine the time to begin modeling; t was set equal to 0 at the time of solute application. The solute was applied in the

Walworth experiments (t = 0) two days after the drain tile discharge had reached a steady state. The depth at which the solute concentration was modeled (x_T) was the depth that the drain tile lines were buried below the surface. At the Walworth field site the drain tiles were buried at approximately 95 cm. The depth of the distribution zone (x_d) was not measured during the experiments or known from any other information. Thus it was set for all of the Walworth experiments to be 10 cm. The depth of the conveyance zone (x_c) was calculated by subtracting the depth of the distribution zone from x_T. The depth of water in the distribution zone (w) was found by multiplying the moisture content of the distribution zone, Θ_d by x_d. The moisture content was not measured for these experiments so it was set to be 0.35 cm^3 cm^{-3} for the lowest irrigation rate at Walworth and assumed to increase with the higher irrigation rates of subsequent experiments. For the intermediate irrigation rate at Walworth Θ_d = 0.40 cm^3 cm^{-3} and for the highest irrigation rate the moisture content was set at saturation (0.45 cm^3 cm^{-3}) because it was reported that any higher irrigation rate caused ponding at the soil surface, this indicates that the entire soil profile was filled to capacity. This increasing depth of water in the distribution zone is consistent with the results from Kim et al. (2005). The area of application, A_a, is the area which the tracer (solute) was applied and I_r is the irrigation rate over the solute applied area, these data were given for each experiment.

After the initial parameters were determined, the fitting parameters were used to adjust the modeled breakthrough curve. These fitting parameters are as follows: the solute velocity in each pore group (v_i), the dispersion coefficient for each pore group (D_i), the water flux through each pore group (q_i), and the number of pore groups (n). A systematic approach

was taken in fitting these four parameters. In the steady state experiments the lowest irrigation rate was modeled first and the first pore group was initially modeled with q_1 equal to the total flux (I_r) and the velocity (v_1) was fit to match the initial arrival of the solute in the drain tile discharge. The dispersion coefficient (D_1) was found from an initial estimate of the dispersivity ratio (D_i/v_i) of 2 cm. The dispersivity was not altered significantly throughout the modeling process and a general set of guidelines were developed herein to specify a range for D_i/v_i as shown below:

$$D_i/v_i < 1 \qquad 0 < v_i < 1 \qquad [L] \tag{15a}$$

$$2 \leq D_i/v_i \leq 5 \qquad 1 < v_i \qquad [L]. \tag{15b}$$

If the modeled breakthrough curve did not fit the measured breakthrough curve well with one pore group, additional pore groups were added and v_i and q_i were adjusted until a reasonable fit was obtained. At each step in this process the sum of each q_i was equal to I_r.

When the next experiment (the intermediate irrigation rate) at Walworth was modeled each of the pore groups used to model the previous (lower) irrigation rate experiment were implemented in the higher irrigation rate model. As discussed in the GPFM Conceptualization section, it is assumed that the slower velocity pore groups (i.e. smaller pore size) fill first and the faster pores subsequently fill until the imposed water flux (irrigation) is satisfied. It is also assumed that the boundary moisture content for each pore group will remain constant for a given soil. As a result, Equations 8, 9, and 10 dictate that the water flux will remain constant if it is assumed that the irrigation rate does not have an effect on the pore water velocity. Following this, the pore groups modeled in the lower irrigation rate experiments maintain the same q_i, v_i, and D_i. The only time this is not true is for the water flux of the

fastest pore group, in a situation as shown in Eq. 9. If the moisture content of the fastest velocity pore group for a given experiment did not reach the boundary moisture content, q_i for the same pore group under a higher irrigation rate will cause the water flux to increase.

The tracer arrival occurred earlier for a higher irrigation rate so additional (higher velocity) pore groups were added as necessary in order to match the arrival of the tracer. If the additional pore group failed to capture the increased activity, further pore groups were added until a satisfactory fit was obtained.

In order to model the SEPAC experiments using the GPFM, procedural modifications had to be made as a result of the transient flow condition and sequentially applied tracers. Under steady state conditions, where the soil remained at the same moisture content throughout the experiment, we could assume that the hydraulic gradient did not change. Under transient conditions the matric potential at the wetting front initially will increase the velocity in the pore group above the steady state rate. In addition after irrigation is stopped the flux ceases in individual pore groups in accordance with the pore velocity. Thus the transient nature was simulated in an ad hoc manner by turning individual pore groups on and off. Consequently, when the irrigation began and the first tracer was applied (at t = 0) not all of the pore groups were contributing to the solute transport (i.e. q_i = 0); whereas, the Walworth experiments began after the system was at steady state causing all applicable pore groups to be active. Initially, the entire water flux was divided between the inactive pores that were immobilizing water (assumed to be in the distribution zone) and a single (low velocity) pore group. The difference between the irrigation rate and the sum of the water flux at any time during

irrigation for each pore group was used to calculate the increased moisture content in the distribution zone. As the soil profile became progressively wetter additional higher velocity pore groups would receive the excess water coming from the distribution zone and eventually become active. A pore group was said to become active at the time it reached a fully flowing condition. The pore group activation time is shown by $_{acti}$ for pore group *i* and the pore group time series is shown by t_{pi}, while *t* is the time series beginning at the start of a given experiment. The pore group time series is calculated by the following:

$$t_{pi} = t - _{acti} \quad (16)$$

The activation times of the pore groups were not known so the pore group activity was based upon the measured drainage from the tile line (i.e. the pore group activation times and water fluxes were fitted to the drain tile discharge as shown in Figure 10). After the irrigation was shut off, the emptying, or the "shut off," time of each pore group was calculated by dividing x_c by v_i. This time was used as the time that q_i for the respective pore group went to zero.

The four sequentially applied tracers could be modeled independently of one another because the tracers were non-reactive and would not have an affect on the transport of one another. Each tracer was assigned an integer value of *h* corresponding to the order of tracer application. For example *h* = 1 for Br and *h* = 4 for 2,6-DFBA. The time series for tracer *h* (t_{th}) was calculated by:

$$t_{th} = t - \tau_{aph} \quad (17)$$

where $_{aph}$ is the time of tracer application and *t* is the overall time counter. Time *t* is equal to 0 at the beginning of the experiment, and for the SEPAC

experiment *t* equivalent to t_{t1} because $_{ap1}$ = 0. In other words, tracer 1 was applied at the same time that the experiment began.

When considering a specific tracer the time series associated with that tracer begins when the tracer is applied. This means that in Equation 1a and where Equation 1a is found in Equations 3 and 7, the time will always be t_{th}. This time series is also used in the remainder of Equations 3 and 7 (which pertain to the conveyance zone transport) providing that the modeled pore groups become active at the same time or prior to the tracer application. However, at times during the SEPAC experiment, tracers were applied before the time that a pore group became active and the tracer later flowed through these pore groups. In this case the time series pertaining to the conveyance zone transport would start at zero when the specific pore group became active. In order to demonstrate this Equation 7 becomes

$$J_i'(x_c,t) = \frac{1}{2} C_o q_i \exp\left(-\frac{I_r}{w} t_{th}\right) \left\{ \begin{array}{l} \exp\left[\frac{v_i x_c}{2D_i}(1-\alpha_i)\right] erfc\left(\frac{x_c - v_i t_{pi}\alpha_i}{2\sqrt{D_i t_{pi}}}\right) \\ + \exp\left[\frac{v_i x_c}{2D_i}(1+\alpha_i)\right] erfc\left(\frac{x_c + v_i t_{pi}\alpha_i}{2\sqrt{D_i t_{pi}}}\right) \end{array} \right\} \quad (18)$$

where t_{pi} (the time series for pore group *i)* and t_{th} (the time series for tracer *h*) are both functions of *t*. The pore group time series is calculated by the following:

$$t_{pi} = t_{th} \qquad \tau_{acti} \leq \tau_{aph} \quad (19a)$$

$$t_{pi} = t - \tau_{acti} \qquad \tau_{acti} > \tau_{aph} \quad (19b)$$

where $_{aph}$ is the time that the pore group becomes active.

The other parameters used to model the sequentially applied tracer experiment from the SEPAC field site were chosen in the same manner as for the Walworth experiment.

RESULTS

Walworth, WI: Steady State Experiments

The initial parameters used to model the Walworth experiments are shown in Table 4 and the pore groups fitted to match the breakthrough curves are shown in Tables 5a, b, and c. Figures 6a, b, and c compare the modeled and measured breakthrough curves from each irrigation rate using three different scenarios. The first of these scenarios (S1) was modeled just as described in the model implementation section above- by fitting the pore groups to the data from the lowest irrigation rate experiment first and then adding additional pore groups for the higher irrigation rates. The second scenario (S2) was conducted identically except the middle irrigation rate data was modeled first. In doing this the lowest irrigation rate data was simultaneously modeled by using a subset of the lower velocity pore groups. This subset begins with the lowest velocity pore group and includes each successive pore group until the sum of q_i is equal to the irrigation rate. After using these pore groups to model the first two irrigation rates, further pore groups were added to model the highest irrigation rate. Following the same procedure, the third scenario (S3) was achieved by modeling the highest irrigation rate experiment first and using the appropriate subset of pore groups (based on the sum of q_i) for the lower irrigation rates. These three scenarios are denoted by S3, S2, and S1 for the data set that each was initially fitted to.

Table 4: Initial parameters for the experiments at Walworth. Each term is stated below.

Primary data set for modeling scenario:	S1	S2	S3	
Irrigation rate (I_r)	0.12	0.24	0.44	cm hr^{-1}
Total depth (x_T)	95	95	95	cm
Distribution zone depth (x_d)	10	10	10	cm
Conveyance zone depth (x_c)	85	85	85	cm
Depth of water in the distribution zone (w)	3.5	4.0	4.5	cm
Area of Tracer Application A_a	168	168	84	m^2
Number of Pore Groups (n)	5	7	10	

Table 5a: The pore groups used to model all three irrigation rates in scenario S1 for Walworth. Pore groups 1-5 were initially used to model the 0.12 cm hr^{-1} irrigation rate. This table points out the irrigation rate (I_r), the pore velocity (v_i), each pore group's dispersion coefficient (D_i), and the water flux for each pore group (q_i).

		I_r (cm hr^{-1})	0.12	0.24	0.44
Pore group	v_i cm hr^{-1}	D_i cm^2 hr^{-1}	q_i	q_i cm hr^{-1}	q_i
10	30	150			0.035
9	15	75			0.04
8	5	15			0.07
7	2.5	5		0.025	0.08
6	2	4		0.08	0.08
5	1.5	3	0.045	0.06	0.06
4	1	1	0.04	0.04	0.04
3	0.7	0.7	0.02	0.02	0.02
2	0.5	0.5	0.01	0.01	0.01
1	0.3	0.15	0.005	0.005	0.005
		q_T (cm hr^{-1})	0.12	0.24	0.44

Table 5b: The pore groups used to model all three irrigation rates in scenario S2 for Walworth. Pore groups 1-7 were initially used to model the 0.24cm/hr irrigation rate. This table points out the irrigation rate (I_r), the pore velocity (v_i), each pore group's dispersion coefficient (D_i), and the water flux for each pore group (q_i).

		Ir (cm hr^{-1})	0.12	0.24	0.44
Pore group	v_i cm hr^{-1}	D_i cm^2 hr^{-1}	q_i	q_i cm hr^{-1}	q_i
11	30	150			0.032
10	12	48			0.04
9	6	12			0.05
8	4	8			0.05
7	3	6		0.022	0.05
6	1.8	3.6		0.04	0.04
5	1.1	2.2	0.032	0.09	0.09
4	0.7	0.7	0.05	0.05	0.05
3	0.5	0.5	0.025	0.025	0.025
2	0.4	0.4	0.009	0.009	0.009
1	0.3	0.15	0.004	0.004	0.004
		q_T (cm hr^{-1})	0.12	0.24	0.44

Table 5c: The pore groups used to model all three irrigation rates in scenario S3 for Walworth. All pore groups were initially used to model the 0.44 cm hr^{-1} irrigation rate This table points out the irrigation rate (I_r), the pore velocity (v_i), each pore group's dispersion coefficient (D_i), and the water flux for each pore group (q_i).

		Ir (cm hr^{-1})	0.12	0.24	0.44
Pore group	v_i cm hr^{-1}	Di cm^2 hr^{-1}	q_i	q_i cm hr^{-1}	q_i
9	30	150			0.045
8	8	40			0.04
7	3.5	10.5			0.08
6	1.9	3.8		0.065	0.10
5	1.2	1.2	0.005	0.06	0.06
4	0.8	0.8	0.06	0.06	0.06
3	0.6	0.6	0.03	0.03	0.03
2	0.5	0.5	0.02	0.02	0.02
1	0.4	0.16	0.005	0.005	0.005
		q_T (cm hr^{-1})	0.12	0.24	0.44

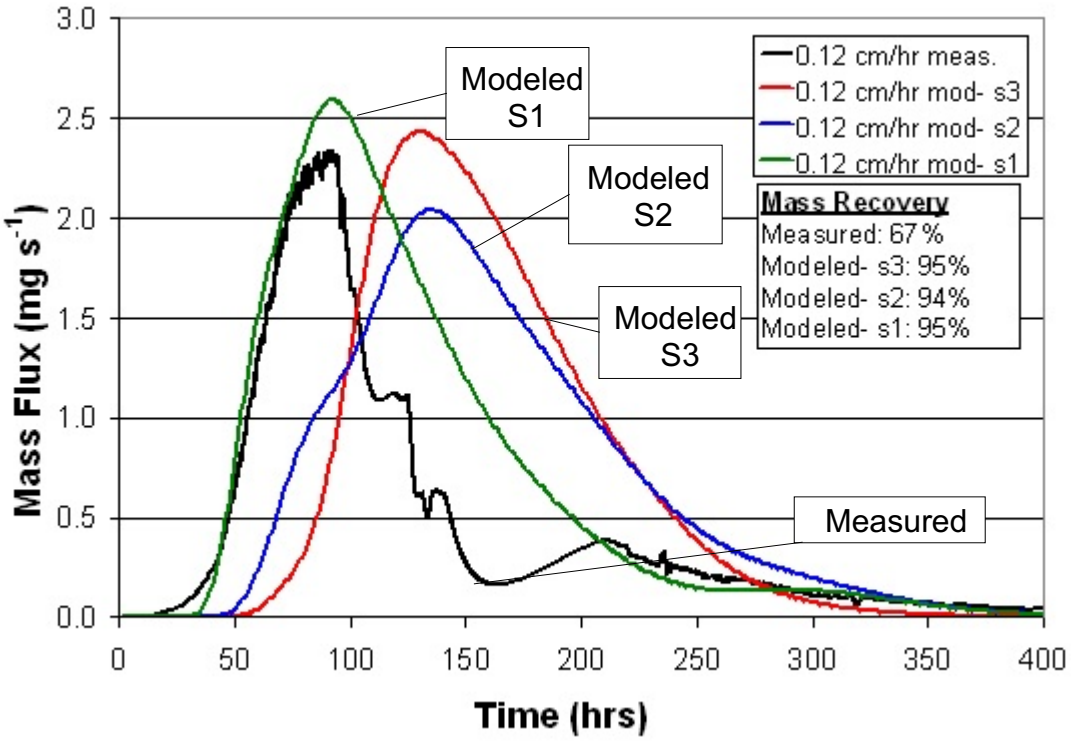

Figure 6a: The results of three modeling scenarios of the 0.12 cm hr^{-1} experiment compared to the measured tracer breakthrough for the same experiment at the Walworth site. The results show the mass flux (mg s^{-1}) of the tracer through the tile line versus the time since the tracer application. S1 is the scenario that was fit directly to the measured data.

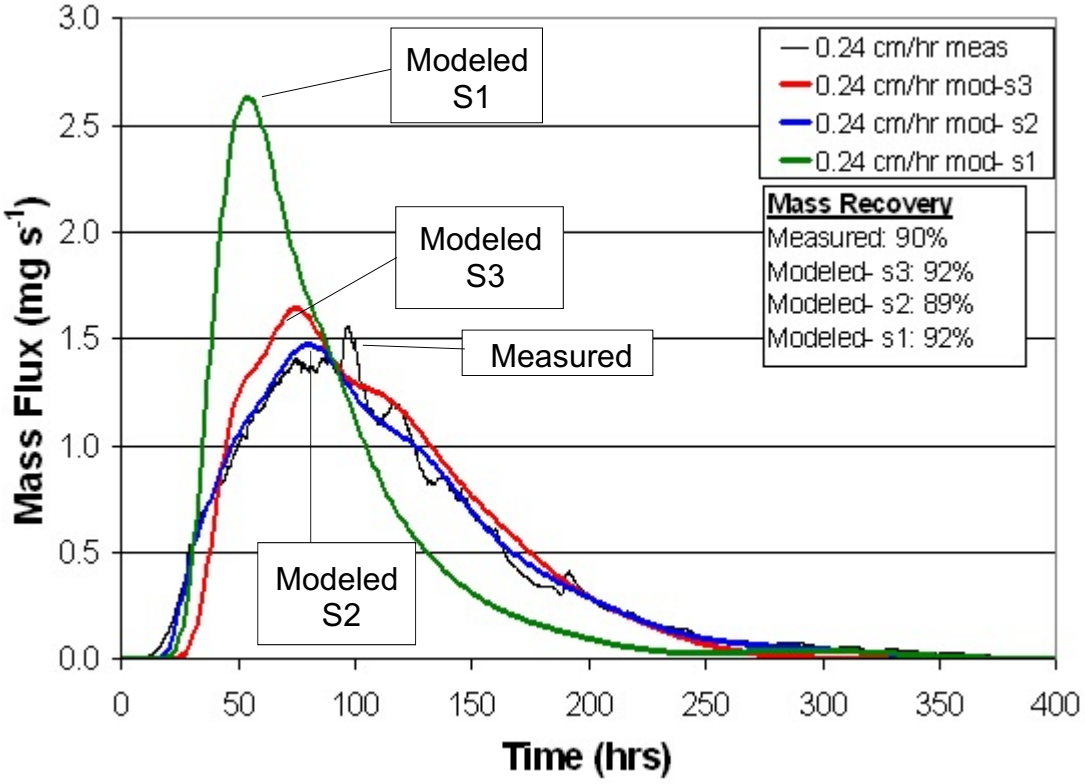

Figure 6b: The results of three modeling scenarios of the 0.24 cm hr^{-1} experiment compared to the measured tracer breakthrough for that experiment at the Walworth site. The results show the mass flux (mg s^{-1}) of the tracer through the tile line versus the time since the tracer application. S2 is the scenario that was fit directly to the measured data.

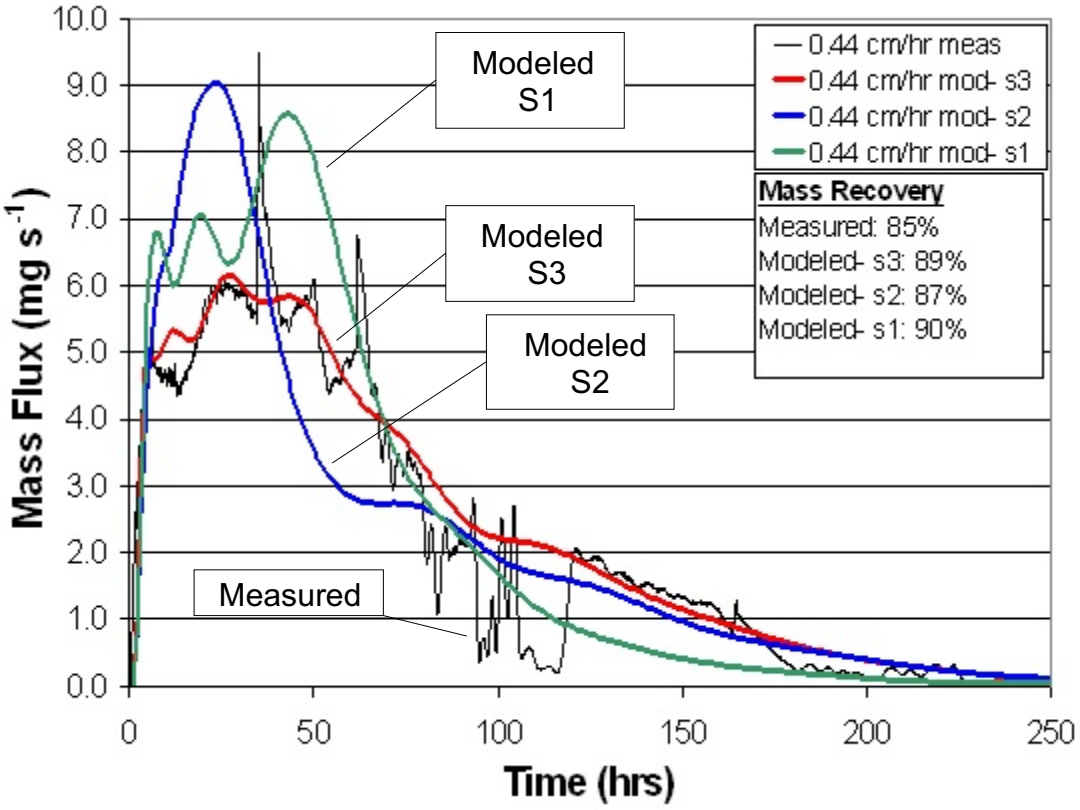

Figure 6c: The results of three modeling scenarios of the 0.44 cm hr^{-1} experiment compared to the measured tracer breakthrough for that experiment at the Walworth site. The results show the mass flux (mg s^{-1}) of the tracer through the tile line versus the time since the tracer application. S3 is the scenario that was fit directly to the measured data.

Five pore groups were used to model the lowest irrigation rate (0.12 cm hr^{-1}) experiment in all three scenarios, shown in Tables 5a, b, and c with the modeled breakthrough curves calculated from these parameters in Figure 6a. The modeled mass recovery for each of these modeling scenarios was 95%, 94%, and 95% for the S3, S2, and S1 scenarios, respectively, while the measured was 67%. Each of the modeled recoveries were approximately equal; however, the measured recovery was significantly lower than the modeled recoveries. This significant difference is partly due to damage sustained to the irrigation and monitoring systems from a severe storm and flooding event that occurred during the experiment (Kung, personal communication 2006). A sharp dip in the measured mass flux occurs near 100 hours and recovers slightly at approximately 200 hours. It is speculated that the modeled breakthrough curve of the S1 scenario, shows a pattern similar to what the measured breakthrough curve would have been, had there not been problems in the data collection.

A comparison of the S1 five pore group model to the best fit single pore group for the lowest irrigation rate experiment is shown in Figure 7a. The single pore group model is the best fit scenario found by adjusting the velocity and dispersion coefficient and setting the water flux equal to the irrigation rate (0.12 cm hr^{-1}). In order to obtain this fit the velocity was set equal to 1.2 cm hr^{-1} and the dispersion coefficient was 3 cm^2 hr^{-1}.

One pore group models the lowest irrigation rate reasonably well, showing that the bulk of the flow under this irrigation rate is representative of the typical “matrix” flow. However, when the same comparison is made for the middle irrigation rate (the best fit single pore group to the S2 scenario for the middle irrigation rate) the fit of one pore group is significantly different than

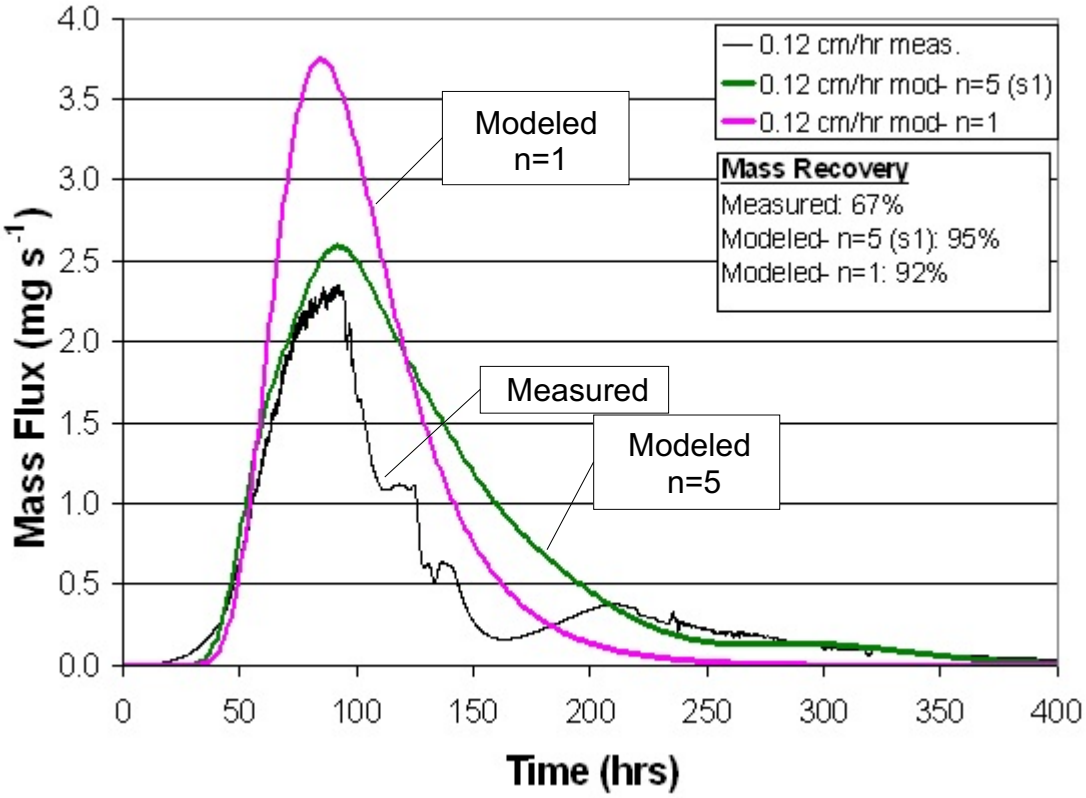

Figure 7a: The model results for using one pore group compared to the S1 scenario (five pore groups) from the 0.12 cm hr^{-1} experiment at Walworth. These two breakthrough curves are shown compared to the measured tracer breakthrough curve for this experiment at the Walworth site. The results show the mass flux (mg s^{-1}) of the tracer through the tile line versus the time since the tracer application.

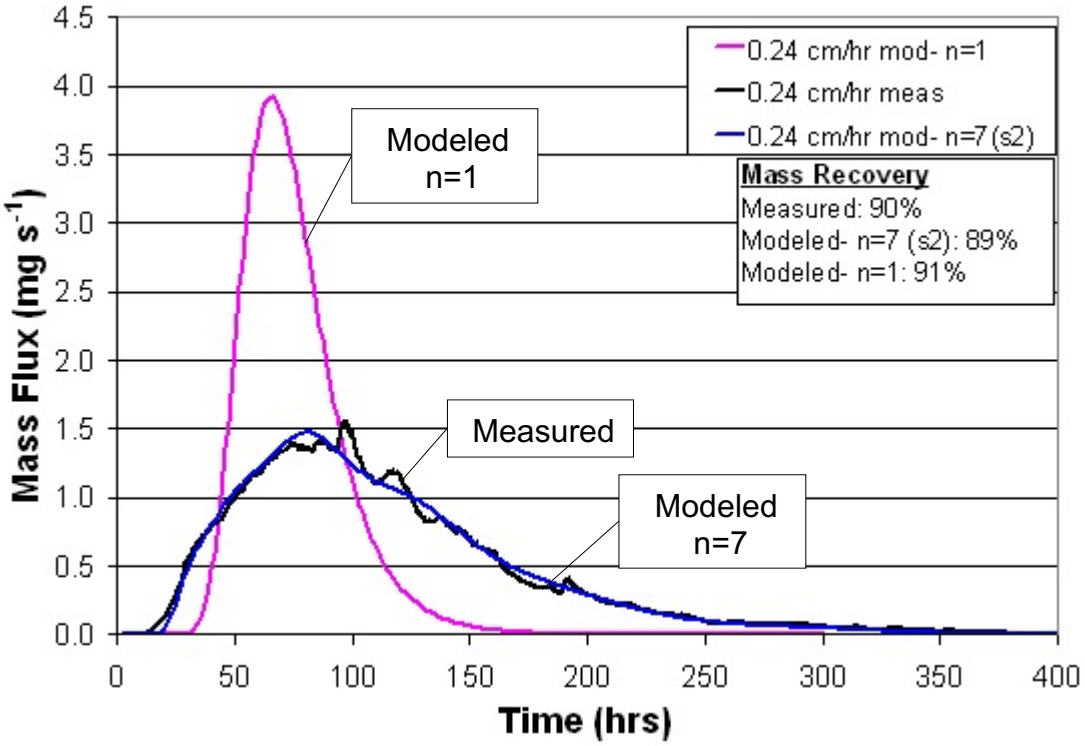

Figure 7b: The model results for using one pore group compared to the S3 scenario (with seven pore groups) from the 0.44 cm hr^{-1} experiment at Walworth. These two breakthrough curves are shown compared to the measured tracer breakthrough curve for this experiment at the Walworth site. The results show the mass flux (mg s^{-1}) of the tracer through the tile line versus the time since the tracer application.

the multiple pore group model, as shown in Figure 7b. It is interesting to note however, that the mass balance did not change significantly. This shows that even though the pattern of the tracer breakthrough is not well represented, the total mass that comes from the drain tile remains essentially the same. A consistent mass balance is essential in modeling and is advantageous in many situations because typically the concern with contaminant transport is the quantity that could potentially reach the groundwater.

An increased irrigation rate results in more water applied at the soil surface causing an overall increase in soil moisture as well as total flow. Therefore, the increase in irrigation rate from 0.12 cm hr^{-1} to 0.24 cm hr^{-1} for the second (middle irrigation rate) experiment activated additional pore groups with higher velocities. The five pore groups used to represent the previous experiment were used in modeling the next higher irrigation rate and maintained the same parameters (e.g. v_i, q_i, and D_i), as seen in Table 5a, b, and c for the respective scenarios.

A total of seven pore groups were used to model the intermediate irrigation rate experiment for the S1 and S2 scenarios and six pore groups were used in the S3 scenario. Figure 6b shows the results from the three scenarios of the 0.24 cm hr^{-1} PFBA experiment. The measured mass recovery was 90% while the modeled was 92%, 89%, and 92% for the S1, S2, and S3 scenarios, respectively. There were no major disturbances when collecting the data shown for this experiment so it was thought to be the most representative of the true behavior of the soil.

The third experiment, with an irrigation rate of 0.44 cm hr^{-1}, caused a significantly faster arrival time and time to peak as can be seen by comparing the measured data of Figure 6c and the measured 0.24 cm hr^{-1} data in Figure

6b. The pore groups used to model this experiment are shown in Table 5a, b, and c. The modeled data from the S1 and S2 scenarios over predict in the first 50-75 hours and under predict after approximately 100 hours. Because the S3 scenario was fitted directly to the highest irrigation rate data, the model shows an exceptional fit to the measured breakthrough curve. During this experiment there were further interruptions due to a severe storm; however, it is difficult to isolate the effects of this extenuating circumstance. The measured mass recovery was approximately 85% and the modeled mass recovery was 90%, 87%, and 89% for the three scenarios (S1, S2, and S3).

The hydraulic conductivity curves developed for each modeled scenario in the Walworth experiments are shown in Figure 8. This relationship is based on the range of moisture content (i.e. $_i$) for a given pore group, and was calculated using the following method from Steenhuis and Parlange (1990):

$$k_i(\Theta) = K_{i-1} + (K_i - K_{i-1})\frac{\Theta - \theta_{i-1}}{\theta_i - \theta_{i-1}}. \qquad (19)$$

As described earlier, Θ is the average moisture content of the soil profile and θ_i is the boundary moisture content for pore group *i*. K_i is the conductivity of pore group *i* at the coinciding boundary moisture content (a constant) while k_i is the conductivity of the specific pore group at moisture content Θ (i.e. observed moisture content). A relationship between the velocity, moisture content, and conductivity was utilized from Steenhuis and Parlange (1990), as shown by:

$$v_i = \frac{K_i - K_{i-1}}{\theta_i - \theta_{i-1}}, \qquad (20)$$

where v_0 = 0. This relationship between the moisture content and the pore group velocities indicates, as would be expected, that the conductivity increases as moisture content increases. Because the pore groups were assumed to behave the same under each irrigation rate, the conductivity curve for a given scenario shows all of the pore groups. In other words, the conductivity curve for the low irrigation rate in any scenario would be the portion of the curve up to the highest velocity pore group that became active for the low irrigation rate experiment.

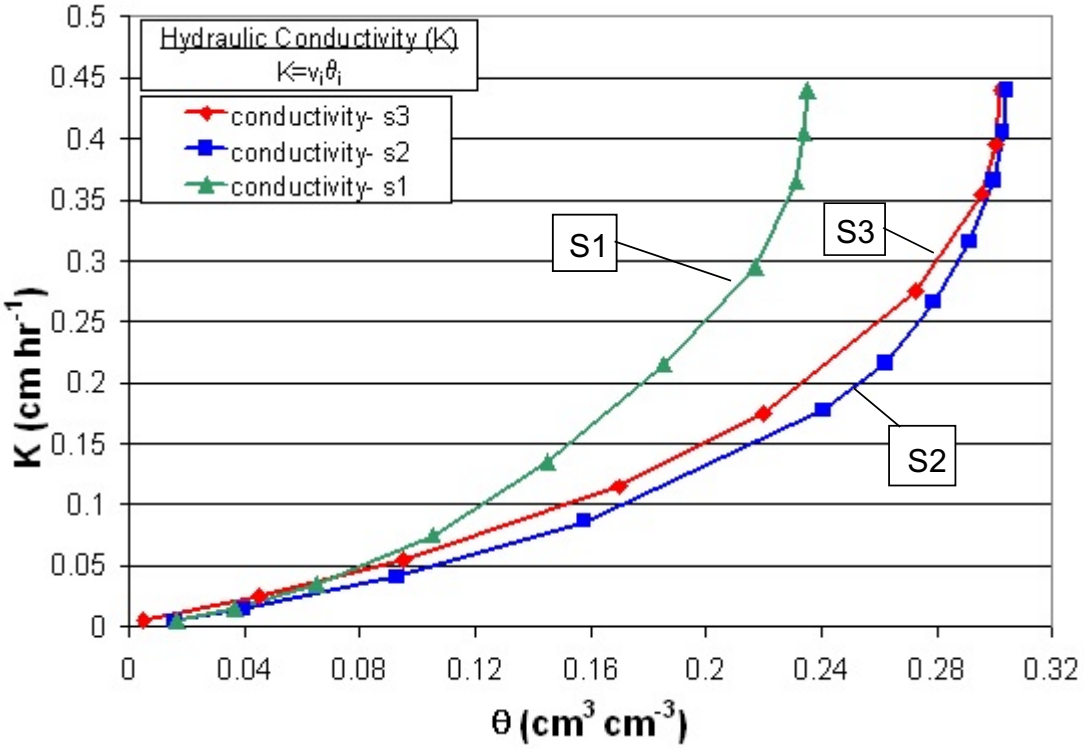

Figure 8: A comparison of the conductivity curves for the modeled scenarios of the Walworth experiments. K (cm hr^{-1}) is the calculated hydraulic conductivity and θ (cm^3 cm^{-3}) is the average moisture content of the soil profile. Each interval, separated by markers on the conductivity curve, is one pore group.

SEPAC, IN: Transient Flow, Sequentially Applied Tracers

Kung et al. (2005) suggested that because of the dramatically decreasing arrival times of the sequentially applied tracers in the SEPAC experiment (from Kung et al. (2000b)), it was clear that there were at least as many active pore groups as there were tracers applied. With this in mind Br (the first tracer applied) was initially modeled with one slow velocity pore group. At t = 2 hrs, when PFBA was applied, a second pore group became active. At this time some of the Br tracer remained in the distribution zone (as governed by Eq. 1a). The remaining Br would consequently be distributed to newly activated pore groups in the conveyance zone. When modeling the second pore group the time of Br application clearly would not change; however, the Br that was routed through pore group number 2 would use the activation time for that pore group in the appropriate places in Eq. 18. This process was followed until all tracers were modeled through all four pore groups. Figure 9 shows a conceptual diagram of the pore groups and the pulses of tracers in each pore group at t = 8 hrs, two hours after the last tracer was applied.

At t = 10 hrs, the time that the irrigation was turned off during the SEPAC experiment, the pore groups would begin to drain. Once the last pulse of water reached the end of the pore groups the active pore groups would become essentially inactive with only a small amount of matrix flow occurring. The drainage time was calculated based on the velocity of the solute and the depth of the soil profile. The drainage time was also limited by the amount of water that was modeled to go into the pore group.

Table 6 shows the fitted parameters for the SEPAC experiment. The depth of the distribution zone was set at 10 cm for each experiment and the

initial moisture content of the distribution zone increased as the irrigation continued causing more soil pores to become active. The difference of the total irrigation rate less the sum of the water flux for the active pores was used to quantify the amount that the moisture content of the distribution zone increased. Upon multiplying this difference by the time interval, a depth of water was obtained that was stored in the soil profile (assumed to be in the distribution zone as the water flow through the conveyance zone was thought to be well established in the pore groups and thereby not available for storage). This depth of water was divided by the depth of the distribution zone, which resulted in the increase in moisture content.

It is also important to note that the water flux (q_i) was constrained so that each tracer was modeled with the same distribution through each pore group. This distribution is shown in Figure 10 as compared to the measured drain tile discharge. The modeled water flux is offset in such a way that it occurs earlier than the tile discharge. This is because the water flux is the water coming from the distribution zone and being routed into the top of each pore group. Whereas, the measured tile discharge comes from the effluent out of the bottom of each pore group.

The modeling results for the SEPAC experiment are seen in Figures 11a, b, c, and d. The first overall impression of these data are that the modeled breakthrough curves show sharp discontinuities. This is a result of the pore groups becoming active and draining (once the irrigation has been turned off) at instantaneous times rather than gradually filling and emptying.

The modeling results for Br in Fig. 11a show a significant over prediction (19% modeled mass recovery compared to 7% measured). The

later applied tracers (Figs. 11b, c, and d) show slightly less significant over prediction.

A conductivity curve was also developed for the SEPAC experiment as shown in Figure 12. Because of the transient nature of the flow during this experiment, this conductivity is a "snapshot" when t = 10 hours. This figure shows that the endpoint of the first pore group is at a moisture content of 0.36 $cm^3\ cm^{-3}$. This, in combination with q_1 reflects the fact that the largest portion of the water flux is going through this low velocity pore group.

Table 6: Modeling parameters for the SEPAC experiment, including the pore group velocities (v_i), pore group dispersion coefficients (D_i), time intervals, the water flux through each pore group (q_i) at each time interval, the modeled depth of the distribution zone (x_d), and the beginning moisture content of the distribution zone (θ) at the time of tracer application.

	PG1	PG2	PG3	PG4				
v_i (cm hr^{-1})	0.5	8	30	60				
D_i (cm^2 hr^{-1})	0.25	16	90	180			x_d (cm)	θ (cm^3 cm^{-3})
Time (hr)	q_i				Total	Tracer		
0-2	0.12	0	0	0	0.12	Br	10	0.260
2-4	0.12	0.06	0	0	0.18	PFBA	10	0.296
4-6	0.12	0.06	0.06	0	0.24	o-TFMBA	10	0.320
6-8	0.12	0.06	0.06	0.06	0.30	2,6-DFBA	10	0.332
8-10	0.12	0.06	0.06	0.06	0.30			
10-11.3	0.12	0.06	0.06	0.06	0.30			
11.3-13.2	0.12	0.06	0.06	0	0.24			
13.2-15.3	0.12	0.06	0	0	0.18			
15.3-20	0.12	0	0	0	0.12			
15.3-20	0	0	0	0	0			

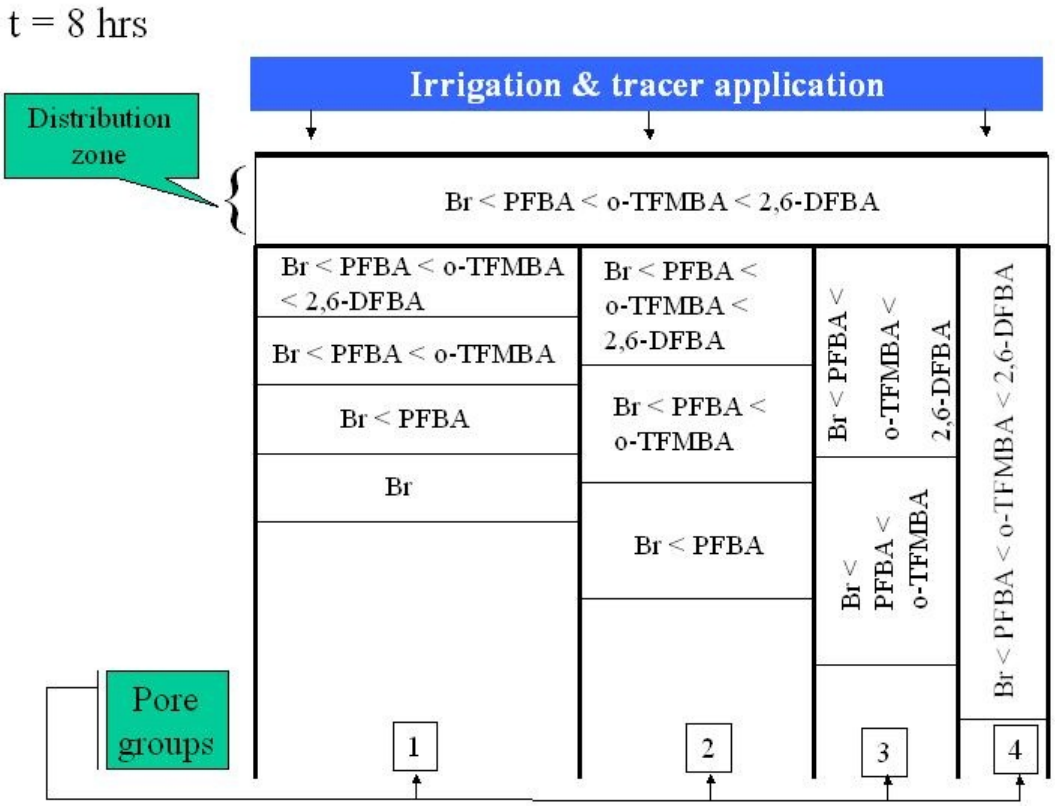

Figure 9: Representation of the modeled pore groups and the relative contribution to the mass flux for each of the sequentially applied tracers from the SEPAC experiment. The distribution zone is called out, below which is the conveyance zone.

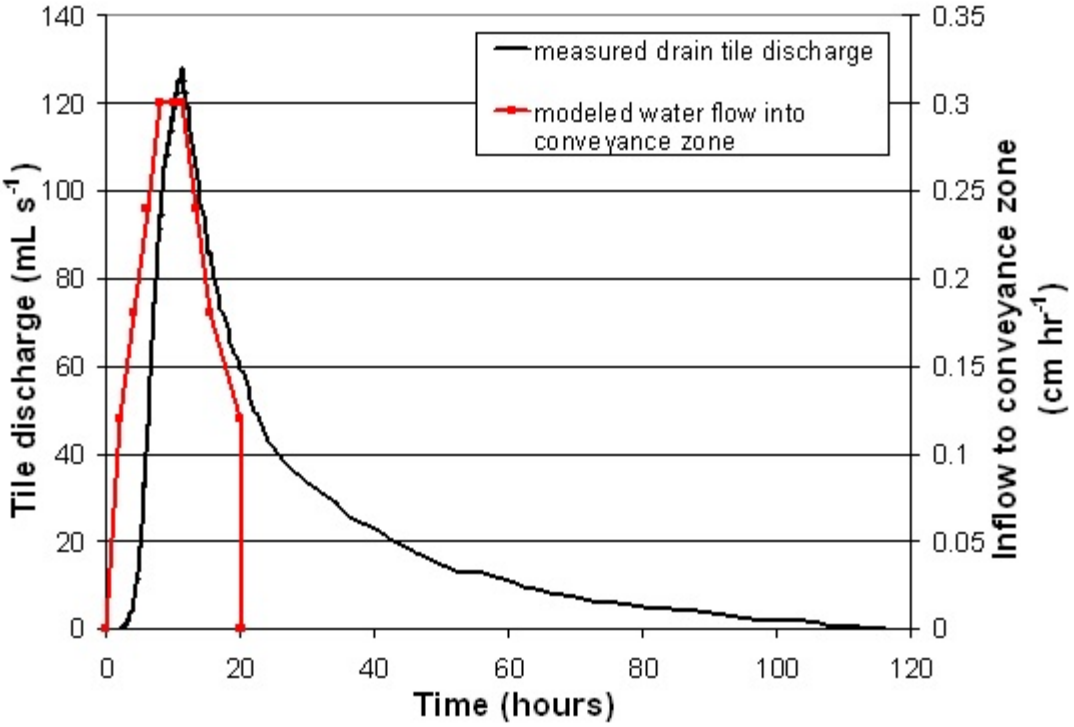

Figure 10: A comparison of the modeled water flux flowing from the distribution zone to the conveyance zone (q_t (cm hr^{-1})) and the measured drain tile discharge (ml s^{-1}) at SEPAC.

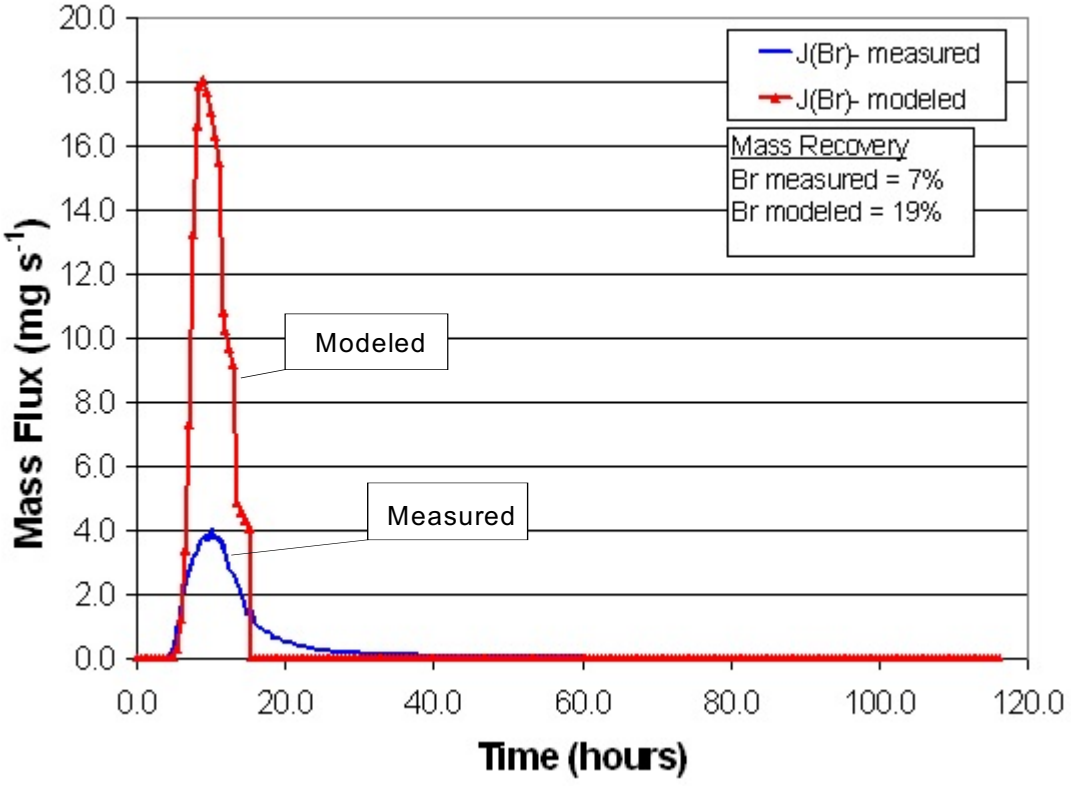

Figure 11a: A comparison of the modeled and measured mass flux for bromide, the first applied tracer (t = 0 hrs) at SEPAC.

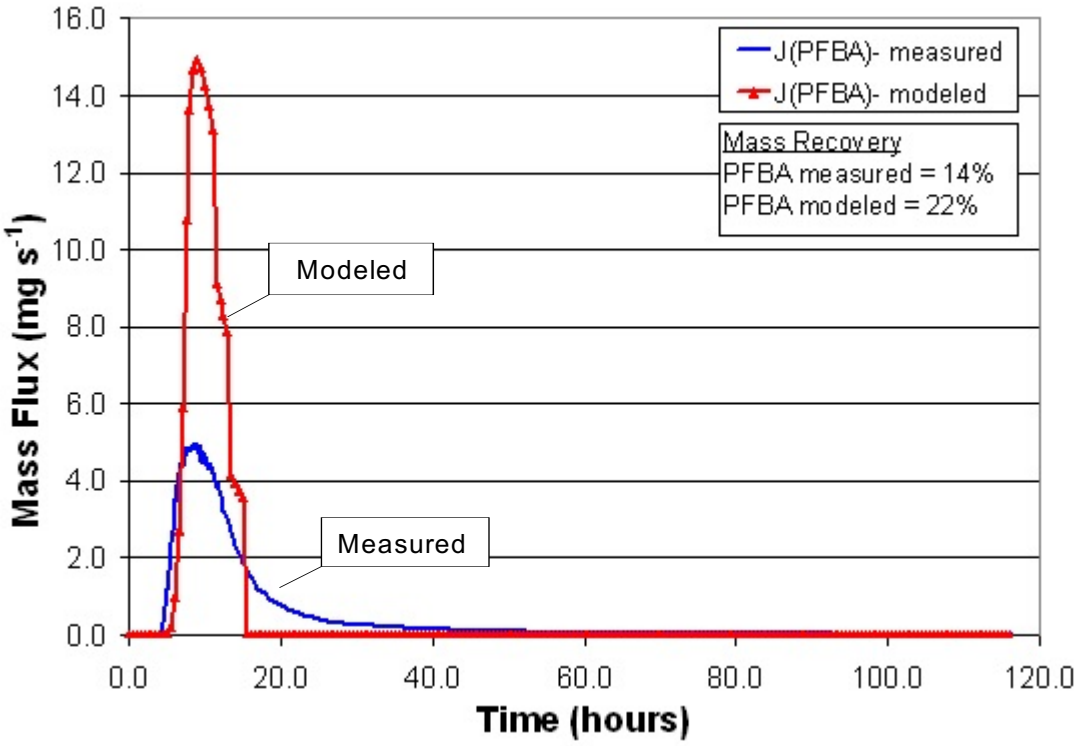

Figure 11b: A comparison of the modeled and measured mass flux for PFBA, the second applied tracer (t = 2 hrs) at SEPAC.

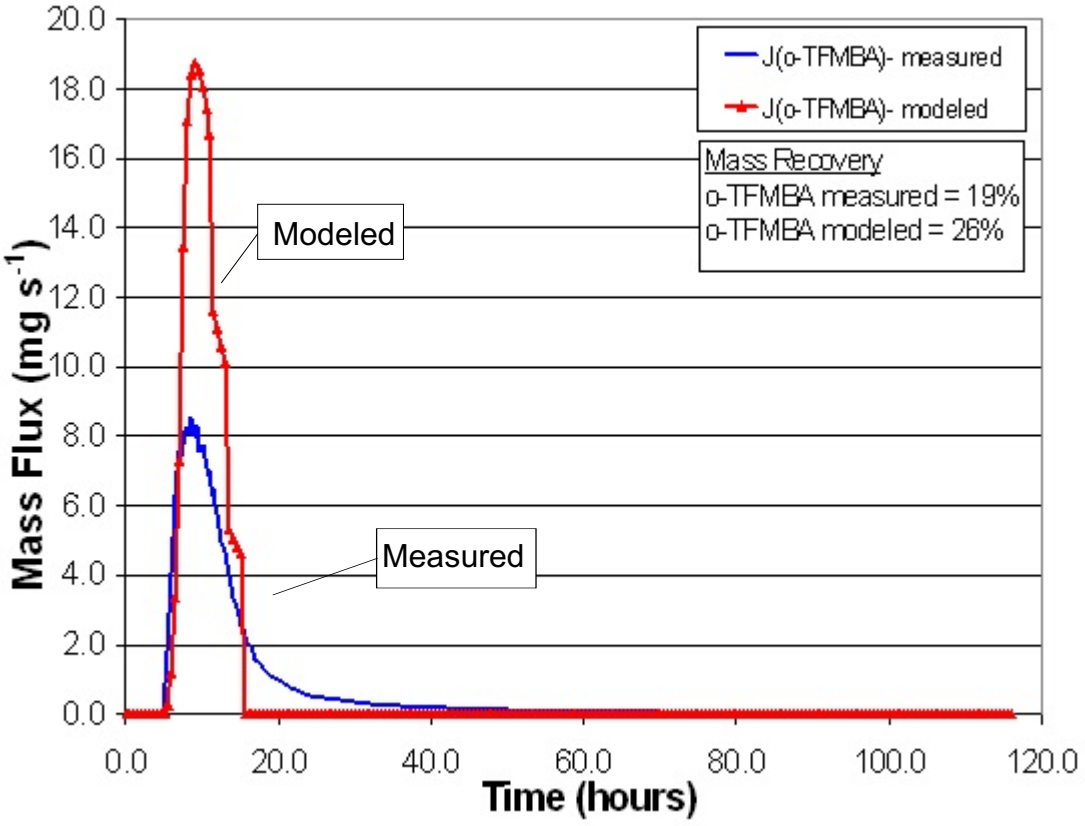

Figure 11c: A comparison of the modeled and measured mass flux for o-TFMBA, the third tracer applied (t = 4 hrs) at SEPAC.

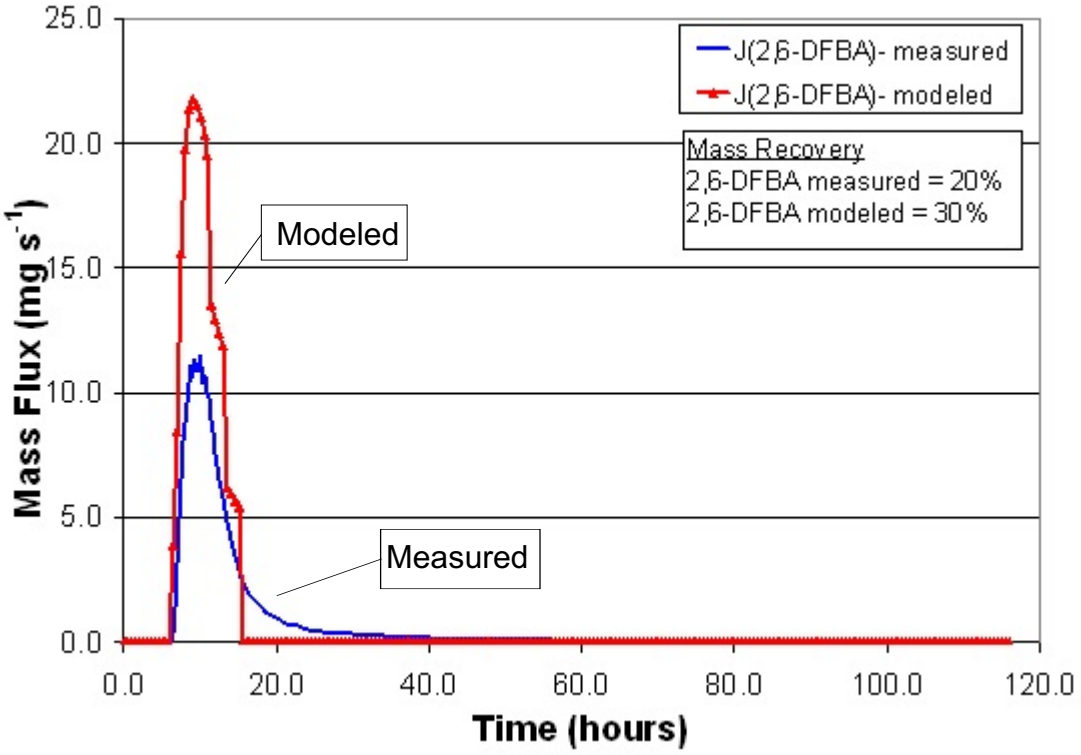

Figure 11d: A comparison of the modeled and measured mass flux for 2,6-DFBA, the fourth tracer applied (t = 6 hrs) at SEPAC.

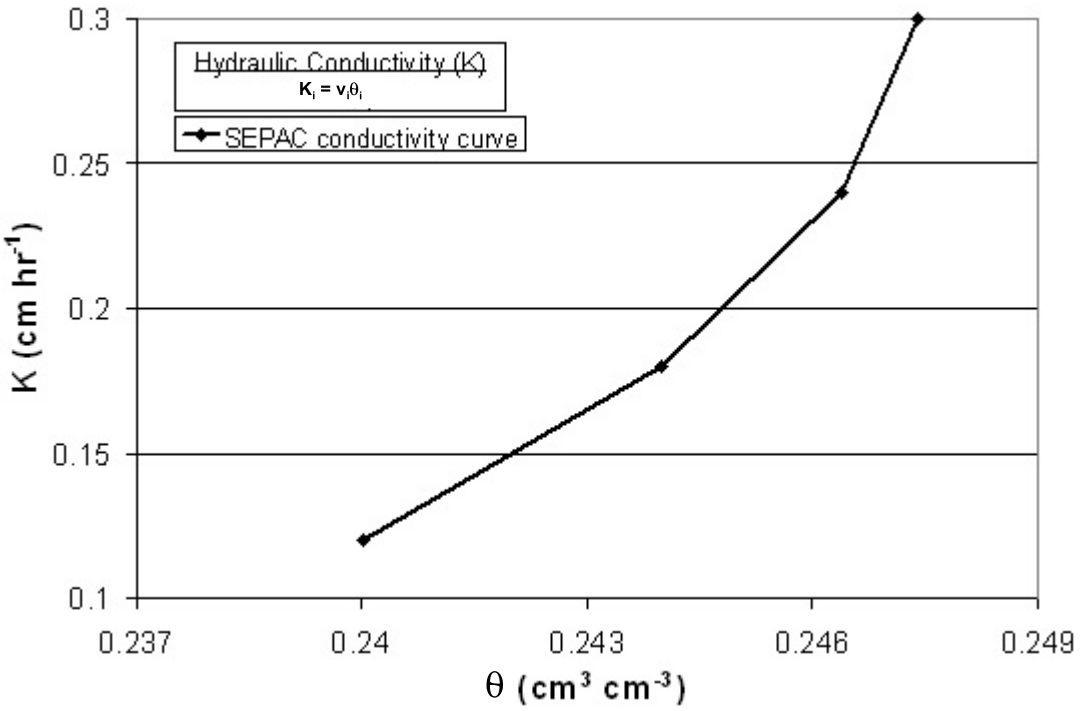

Figure 12: The conductivity curve for the four pore groups modeled at SEPAC. The four points along the curve denote the highest hydraulic conductivity (K [cm hr^{-1}]) and the average moisture content (θ [cm^3 cm^{-3}]) for the soil profile.

DISCUSSION

Walworth, WI: Steady State Experiments

The procedures used to conduct the experiments at the Walworth site provided a method for observing the influence of the entire pore spectrum on solute transport. The high percent recovery (90.3%) for the 0.24 cm hr^{-1} PFBA experiment shows that all pores filling with incoming irrigation water at the time of solute application played a role in transporting the tracer. The ability to model these data and obtain a breakthrough curve that closely resembles the measured breakthrough curve while matching the mass recovery is remarkable. This agreement suggests that the parameters used to model the assigned pore groups are a reasonable average of a similarly behaving group of actual pores. However, when comparing the modeled and measured breakthrough curves of each scenario it is clear that there are differences between the S1, S2, and S3 scenarios, contrary to the expected results. In each scenario the model fit the experiment used to initially set the modeling parameters significantly better than the same experiment in other scenarios (i.e. the S1 scenario showed the best fit for the lowest irrigation rate experiment). If the pore groups behaved as assumed, the best fit parameters for a given pore group would be the same regardless of which data the parameters were derived from. The pore groups are modeled to behave consistently by fixing the amount of water flowing through a specific pore group (q_i) for each irrigation rate during a modeling scenario.

The best fit scenario when comparing the measured and modeled data across all three irrigation rates was the S3 scenario. This scenario showed good results for the highest irrigation rate as would be expected since the parameters were set using the highest irrigation rate data. Aside from missing

the initial arrival of the solute in the middle irrigation rate experiment, the S3 scenario also modeled the middle irrigation rate data well. The S3 scenario did not accurately reproduce the lowest irrigation rate experiment; however, the only scenario to match this data was S1. However, the S3 scenario did show a very similar trend in the predicted breakthrough curve aside from a significantly delayed solute arrival.

It is interesting to note that in the Walworth results the 0.12 cm hr^{-1} and 0.24 cm hr^{-1} experiments were modeled with a peak velocity of approximately one order of magnitude higher than the irrigation rate. The 0.44 cm hr^{-1} irrigation rate had a high velocity that was slightly less than 100 times the irrigation rate. This indicates the relative magnitude of the preferential flow for the highest irrigation rate experiment. It is also interesting to note that for each modeling scenario, at a specific irrigation rate, it is apparent that the shape of the predicted breakthrough curves is significantly different but the mass recoveries are approximately the same. This shows that the mass balance is upheld when using the GPFM regardless of the primary modeling parameters (v_i, D_i, and q_i). These parameters simply affect the shape of the curve.

It is important to note that the moisture content of the distribution zone increased as the irrigation rate increased. The equilibrium depth of water (w) in the distribution zone affects how the solute is released into the conveyance zone: A distribution zone with a large w mitigates the peak height of the solute pulse and causes it to be more disperse (a wider breakthrough curve). Whereas, a small w in the distribution zone transmits the solute to the conveyance zone more rapidly and results in a high sharp peak with less dispersion. However, the irrigation rate (or q_T) has an even larger, and

opposite, impact. This is why the modeled breakthrough curves from the high irrigation rate (which has a larger *w* and irrigation rate) experiment show more peaks.

The hydraulic conductivity curve developed demonstrates the relationship between two of the three main modeling parameters. The established relationship shows the proportion of flow, translated into a moisture content, as it relates to the pore group velocity. The derived curve shows an expected relationship of a measured hydraulic conductivity curve and reflects the high conductivity of the preferential flow paths. This relationship may be a valuable tool in determining the modeling parameters.

SEPAC, IN: Transient Flow, Sequentially Applied Tracers

The SEPAC experiments provide a method for examining the transient processes of solute transport. There are significant differences between steady state flow and a transient situation. However, a good model should work in transient situations as this is typically the case when examining realistic scenarios.

It was found that in transient situations the solute flux is largely influenced by the water flow dynamics. If the water hydrograph from a site is obtainable, the relationship shown in Figure 10 can aid in determining q_i. When looking at the modeled tracer breakthrough curves from SEPAC there is evidence of an over prediction of total mass for the tracers. For the first tracer, this is likely caused by an initial abstraction of water and solutes into the inactive (or very slow) pores, a result of applying the tracer to a soil profile with a moisture deficit (especially in the upper layers). As the pores are filled by incoming water, less abstraction of the successive tracers would occur,

resulting in higher mass recoveries. This concept is supported by the increasing mass recoveries and the significantly decreasing arrival times reported by Kung et al. (2000b). This hypothesis holds true for the modeled results of the first three tracers. However, the modeled results for the final tracer over-predict the mass recovered by nearly as much as the first tracer. It is not clear why this occurs.

The effects of the transient dynamics and short duration irrigation are clearly seen when comparing the measured percent mass recoveries to those from the steady state experiments at the Walworth site. The mass recovery at SEPAC ranged from 7% (for Br^-) to 20% (for 2,6-DFBA) and at Walworth as high as 90%.

The distribution of q in Table 6 reflects the transient behavior in many ways. Initially, all of the water coming into the conveyance zone from the distribution zone above was flowing into the slowest pore group. The slow velocity (small pore size) pore group has an initially high suction potential and is therefore able to absorb the bulk of the irrigation water coming from the distribution zone. However, as this suction potential begins to equalize and additional pore groups become active, the total water flux is distributed to other pore groups. Once the irrigation is shut off at t_o = 10 hours, the remaining water in each pore group continues to flow downward through the pores until the resident water flows out and into the drain tile. At this point q_i goes to zero. The pore group velocities dictate the sequential draining times. The total water flux during this time is equal to the flux from the pore groups that are still in the draining phase.

Inter-site Comparison

It is interesting to note that the tracer arrival time for the highest irrigation rate at Walworth (16 min) and the last applied tracer at SEPAC (18 min) are approximately the same in spite of the varying irrigation rates, durations, and site properties. An additional experiment conducted by Kung et al. (2000a) used similar experimental techniques but a significantly different site, irrigation rate, and a strongly adsorbed tracer and still showed a similarly fast arrival (13 min) of the tracer. This site was in Willsboro, New York and employed the use of rhodamine water tracer. This similarity in arrival times shows the potential for relationships to be made between different sties and may help in developing a method of specifying unknown parameters.

CONCLUSIONS

The Generalized Preferential Flow Model does not require specialized computer software and is sufficiently simple to allow user modification of the model to fit a specific system. However, while possible to model, the introduction of multiple solutes applied at different times in a transient situation provides a challenging and somewhat convoluted modeling approach.

A simple yet effective model such as this is appealing for use as a risk indicator for groundwater contamination. Although the exact arrival times and pattern of the chemical breakthrough was not always completely accurate, there was reasonable accuracy (often within 5%) in predicting the total mass leached through the soil profile. Total chemical mass introduced to groundwater is extremely important in assessing the groundwater quality with respect to regulatory limits.

Results herein indicate that the number of pore groups required to effectively model various scenarios depends on the duration and intensity of irrigation. The SEPAC experiment, with a 10 hour duration of 0.3 cm hr^{-1} irrigation, only required four pore groups; whereas, the Walworth experiment, with over 20 days of 0.44 cm hr^{-1} irrigation required up to eleven pore groups. While an exact number of discrete pore groups is not known for a given situation, a general idea can be obtained by assuming a rapid initial arrival time (15-20 min., as noted above at a depth of one meter) and then modeling sequentially slower velocity pore groups in an effort to reduce gaps between pore group contributions. A general idea of the number of active pore groups will help to characterize solute transport with a level of accuracy that can help identify areas that are high risk for groundwater contamination.

A further challenge in modeling solute transport is to develop a method for finding the solute velocities for each pore group. With this, the multi-domain GPFM will be a viable tool for modeling solute transport in many situations. The ability to model these chosen scenarios shows the capabilities of the convective-dispersive equation in the form of the GPFM and is a good indicator that the processes are satisfactorily conceptualized. This information, in conjunction with the Kung et al. (2005) pore spectrum model, could enhance the accuracy in modeling when dividing the continuous pore spectrum into discrete groups.

REFERENCES

Beven, K. and P. Germann. 1982. Macropores and water-flow in soils. Water Resour. Res. 18:1311-1325.

Darnault, C.J.G., T.S. Steenhuis, P. Garnier, Y.J. Kim, M.B. Jenkins, W.C. Ghiorse, P.C. Baveye and J.Y. Parlange. 2004. Preferential flow and transport of cryptosporidium parvum oocysts through the vadose zone: Experiments and modeling. Vadose Zone Journal 3:262-270.

Dekker, L.W. and C.J. Ritsema. 1994. Fingered flow: The creator of sand columns in dune beach sands. Earth Surf. Processes Landforms 19:153-164.

Durner, W. and H. Fluhler. 1996. Multi-domain model for pore-size dependent transport of solutes in soils. Geoderma 70:281-297.

Feyen, J., D. Jacques, A. Timmerman and J. Vanderborght. 1998. Modelling water flow and solute transport in heterogeneous soils: A review of recent approaches. J. Agric. Eng. Res. 70:231-256.

Fox, G.A., R. Malone, G.J. Sabbagh and K. Rojas. 2004. Interrelationship of macropores and subsurface drainage for conservative tracer and pesticide transport. J. Environ. Qual. 33:2281-2289.

Gish, T.J., K.J.S. Kung, D.C. Perry, J. Posner, G. Bubenzer, C.S. Helling, E.J. Kladivko and T.S. Steenhuis. 2004. Impact of preferential flow at varying irrigation rates by quantifying mass fluxes. J. Environ. Qual. 33:1033-1040.

Hanke, M., D. Perry, K.J.S. Kung and G. Bubenzer. 2004. A low-intensity, high-uniformity water application system. Soil Sci. Soc. Am. J. 68:1833-1837.

Hawes, N.W., B.S. Das, and P.S.C. Rao. 2004. Dual-Domain Solute Transfer and Transport Processes: Evaluation in Batch and Transport Experiments. J. Contam. Hyd. 75: 257-280.

Hill, D.E. and J.Y. Parlange. 1972. Wetting front instability in layered soils. Soil Science Society of America Proceedings 36:697-&.

Jaynes, D.B., S.I. Ahmed, K.J.S. Kung and R.S. Kanwar. 2001. Temporal dynamics of preferential flow to a subsurface drain. Soil Sci. Soc. Am. J. 65:1368-1376.

Kim, Y.J., C.J.G. Darnault, N.O. Bailey, J.Y. Parlange and T.S. Steenhuis. 2005. Equation for describing solute transport in field soils with preferential flow paths. Soil Sci. Soc. Am. J. 69:291-300.

Kung, K.J.S., T.S. Steenhuis, E.J. Kladivko, T.J. Gish, G. Bubenzer and C.S. Helling. 2000a. Impact of preferential flow on the transport of adsorbing and non-adsorbing tracers. Soil Sci. Soc. Am. J. 64:1290-1296.

Kung, K.J.S., E.J. Kladivko, T.J. Gish, T.S. Steenhuis, G. Bubenzer and C.S. Helling. 2000b. Quantifying preferential flow by breakthrough of sequentially applied tracers: Silt loam soil. Soil Sci. Soc. Am. J. 64:1296-1304.

Kung, K.J.S., M. Hanke, C.S. Helling, E.J. Kladivko, T.J. Gish, T.S. Steenhuis and D.B. Jaynes. 2005. Quautifying pore-size spectrum of macropore-type preferential pathways. Soil Sci. Soc. Am. J. 69:1196-1208.

Larsbo, M., S. Roulier, F. Stenemo, R. Kasteel, and N. Jarvis. 2005. An Improved Dual-Permeability Model of Water Flow and Solute Transport in the Vadose Zone. Vadose Zone J. 4: 398-406.

Lawes, J.B., J.H. Gilbert and and R. Warington. 1882. On the amount and composition of the rain and drainage water collected at rothamstead. J. Royal Agr. Soc. of England XVII; XVIII:241-279, 311-350; 1-71.

Parlange, J.Y. 1972. Theory of water movement in soils .4. 2 and 3-dimensional steady infiltration. Soil Sci. 113: 96-101.

Parlange, J.Y. and D.E. Hill. 1976. Theoretical-analysis of wetting front instability in soils. Soil Sci. 122:236-239.

Philip, J.R. 1975. Growth of disturbances in unstable infiltration flows. Soil Sci. Soc. Am. J. 39:1049-1053.

Raats, P.A.C. 1973. Unstable wetting fronts in uniform and nonuniform soils. Soil Sci. Soc. Am. J. 37:681-685.

Richard, T.L. and T.S. Steenhuis. 1988. Tile Drain Sampling of Preferential Flow on a Field Scale. J. Contam. Hydrol. 3:307-325.

Skopp, J. 1981. Microporosity, mesoporosity, and macroporosity of soil - comment. Soil Sci. Soc. Am. J. 45:1246-1246.

Skopp, J., W.R. Gardner and E.J. Tyler. 1981. Solute movement in structured soils - 2-region model with small interaction. Soil Sci. Soc. Am. J. 45:837-842.

Stagnitti, F., J.-. Parlange, T.S. Steenhuis, B. Nijssen and D. Lockington. 1994. Modeling the migration of water soluble contaminants through preferred paths in the soils. p. 367-379. In K. Kovar, J. Soveri (ed.) Groundwater quality management, Tallinn, Estonia. 6-9 September 1993 1994. Wallingford : International Association of Hydrological Sciences Press, Oxfordshire, UK.

Steenhuis, T.S. and J.-Y. Parlange. 1990. Preferential Flow in Structured and Sandy Soils. Engineering: Cornell Quarterly 25:7-14.

Steenhuis, T.S., T.L. Richard, M.B. Parlange, S.O. Aburime, L.D. Geohring and J.Y. Parlange. 1988. Preferential flow influences on drainage of shallow sloping soils. Agric. Water Manage. 14:137-151.

Steenhuis, T.S., J.Y. Parlange, M.B. Parlange and F. Stagnitti. 1988. A simple-model for flow on hillslopes. Agric. Water Manage. 14:153-168.

Steenhuis, T.S., J.Y. Parlange and M.S. Andreini. 1990. A numerical-model for preferential solute movement in structured soils. Geoderma 46:193-208.

Steenhuis, T.S., J. Boll, G. Shalit, J.S. Selker and I.A. Merwin. 1994. A simple equation for predicting preferential flow solute concentrations. J. Environ. Qual. 23:1058-1064.

Toride, N., F.J. Leij and and M.Th. van Genuchten. 1995. The CXTFIT code for estimating transport parameters from laboratory or field tracer experiments. version 2.0. Rep. 137. U.S. Salinity Laboratory, Riverside, CA.

Van der Molen, H.W. 1956. Van der molen, H. W.; 1956. desalinization of saline soils as a column process. soil sci. 81:19-27. Soil Sci. 81:19-27.

Wycisk, P., H. Weiss, A. Kaschl, S. Heidrich and K. Sommerwerk. 2003. Groundwater pollution and remediation options for multi-source contaminated aquifers (Bitterfeld/Wolfen, germany). Toxicol. Lett. 140:343-351.